STRUCTURAL BIOLOGY

Volume 78 (2022)

Supporting information for article:

Evaluating the impact of X-ray damage on conformational heterogeneity in room-temperature (277 K) and cryo-cooled protein crystals

Filip Yabukarski, Tzanko Doukov, Daniel A. Mokhtari, Siyuan Du and Daniel Herschlag

S1. Room temperature X-ray diffraction data collection.

Room temperature (RT) diffraction data from protein crystals can be obtained at either synchrotron X-ray beamlines or at X-ray free electron lasers (XFELs) facilities. (Although home X-ray sources are still in use, the vast majority of experiments are currently not conducted using home sources.) In particular, serial crystallography using XFELs enabled the collection of diffraction data that is essentially X-ray damage-free (Chapman *et al.*, 2011; Doerr, 2011; Neutze *et al.*, 2000). Nevertheless, this approach is not limitation-free: obtainable diffraction resolutions tend to be lower when compared to resolutions obtained at synchrotron beamlines, data collection often requires complex sample delivery instrumentation (e.g., for a crystal slurry), and instrument availability is currently limited. Recent technical and instrumental developments have led to the development of the serial synchrotron crystallography (SSX) technique, which combines both traditional synchrotron data collection with serial diffraction data collection from large number of small crystals, but these datasets are not X-ray damage-free, as is the case for any non-XFEL data collection approach (de la Mora *et al.*, 2020).

S2. X-ray damage in protein crystals.

X-ray damage can be described as global, the overall decay of diffraction intensity, and specific, the chemical changes in proteins that are directly related to changes in structure (Garman, 2010; Holton, 2009; Nave & Garman, 2005). Global X-ray damage occurs at all temperatures, but the X-ray dose required to halve the diffraction intensity is typically 50-100 times lower at RT than at cryo temperatures (Roedig *et al.*, 2016; Southworth-Davies *et al.*, 2007; Warkentin *et al.*, 2011; Warkentin & Thorne, 2010). Commensurate with the pervasive use of cryo cooling in X-ray crystallography, there have been numerous studies of X-ray damage under these conditions (Burmeister, 2000; Carugo & Carugo, 2005; Fioravanti *et al.*, 2007; Garman, 2010; Weik *et al.*, 2000). At cryo temperatures, specific X-ray damage generally occurs before substantial overall diffraction intensity decay, and X-ray damage can alter structural details, the most commonly observed of which are disulfide bond reduction, decarboxylation of acidic side chains, and modifications at metallo-centers, with active site residues suggested to be particularly sensitive (Burmeister, 2000; Carugo & Carugo, 2005; Fioravanti *et al.*, 2007; Garman, 2010; Ravelli & McSweeney, 2000; Weik *et al.*, 2000). The effects of specific X-ray damage at RT have been less studied, but recent work generally points to less specific X-ray damage relative to cryo temperatures (Gotthard *et al.*, 2019; Roedig *et al.*, 2016; Russi *et al.*, 2017). Alternatively, or in addition, it is possible that at RT X-ray damage causes the crystal lattice to collapse before specific damage can be observed, contrasting data collection from cryo-cooled crystals where specific damage occurs before crystal lattice deterioration.

S3. Assessing disulfide bond X-ray damage at room temperature.

Disulfide bonds are exquisitely sensitive to X-ray damage. At cryo temperatures specific damage to disulfide bonds, such as breaking the disulfide bond as illustrated in **Figure 3D** often appears before other X-ray damage effects can be observed in electron density maps (Burmeister, 2000; Leiros *et al.*, 2001; Ravelli & McSweeney, 2000). To evaluate the extent to which disulfide bonds are X-ray damaged with increasing absorbed X-ray doses at room temperature, we compared the *Ringer* profiles and the electron density maps for each of the 26 disulfide bond-forming cysteine residues (13 disulfides) in all three proteins (**Figure S8**). The 2Fo-Fc electron density maps (1σ, grey mesh) for the least *vs.* the most X-ray damaged datasets were highly similar in all cases, the associated Fo-Fc electron density maps (3σ, green and red mesh for positive and negative density peaks, respectively) were featureless, and the corresponding *Ringer* profiles were highly similar in all cases, with $P_{CC} \geq 0.997 \pm 0.002$ in all cases (average and standard deviation, respectively). To more thoroughly assess potential differences due to X-ray damage, we calculated difference Fo-Fo electron density maps between the least and most damaged datasets for each protein (**Figure S9**). Inspection of these maps reveals a stronger than average negative feature and thus unambiguous damage in one case, C121-C193 in thaumatin (**Figure S9**), a disulfide bond within a region that was previously identified as highly sensitive to X-ray damage (Warkentin *et al.*, 2012). However, even in this case, the damage is modest; it could not be identified via inspection of conventional 2Fo-Fc and Fo-Fc maps alone and did not lead to the detectable appearance of new rotameric states. Focusing on the C6-C127 and C76-C94 disulfide bonds in lysozyme, previously identified as the two most susceptible to X-ray damage disulfide bonds in cryo-cooled lysozyme crystals (Ravelli & McSweeney, 2000), we observed no indication of damage for the former and minor damage features (Fo-Fo difference electron density, **Figure S9**) present for the later that could originate from minor direct damage, consistent with spectroscopic evidence for X-ray damage-induced changes in lysozyme disulfide bond vibration at room temperature, presumably due to S-S bond lengthening (Gotthard *et al.*, 2019; Ravelli & McSweeney, 2000; Weik *et al.*, 2002). The X-ray damage effects to disulfides that we observed were generally of the same magnitude as features observed at other random sites, again consistent with prior observations suggesting that at RT specific chemical damage could appear as randomly as global damage (Gotthard *et al.*, 2019). On the other hand, in thaumatin the Fo-Fo difference electron density map features for the C56-C66 disulfide are indicative of an elongation of the bond (**Figure S9**), consistent with previous observations of disulfide bond elongation caused by X-ray damage (Gotthard *et al.*, 2019; Ravelli & McSweeney, 2000; Weik *et al.*, 2002). For the other residues, peaks around disulfide bonds in difference Fo-Fo maps were weak and similar in magnitude to peaks throughout the entire map. Overall, our results provide evidence that some X-ray damage occurred to disulfide bonds in our datasets but that the damage was generally not more prominent than damage observed at non-disulfide sites (**Figures S8-S9**). These results are consistent with recent

studies at RT that found X-ray damage to disulfides (de la Mora *et al.*, 2020; Gotthard *et al.*, 2019; Russi *et al.*, 2017) and provide evidence for similar dose scales for specific and global X-ray damage evolution. Nevertheless, despite evidence for minor X-ray damage in the difference electron density maps, the *Ringer* analysis showed no evidence for changes in rotameric populations for disulfide bond-forming cysteine residues, including for the C121-C193 bond which presented the strongest difference Fo-Fo features (**Figure S9**), within the limits of X-ray damage explored in this work.

Previous studies provided evidence both for and against X-ray associated damage at disulfide bonds at RT (Coquelle *et al.*, 2015; de la Mora *et al.*, 2020; Gotthard *et al.*, 2019; Roedig *et al.*, 2016; Russi *et al.*, 2017; Southworth-Davies *et al.*, 2007), but the origin of these conflicting results remains unknown. Why do disulfide bonds appear more or less damaged in different RT studies? Based on multi-crystal averaged increasingly X-ray damaged datasets Russi et al. proposed that the amount of damage to a specific site might be different at different X-ray dose rates and that data collected at high dose rates might result in more extensive site-specific damage (Russi *et al.*, 2017). Thus, differing reports about X-ray damage to disulfide bonds at RT could be due to the different extent of disulfide bond breaking being caused by the range of X-ray dose rates employed in different studies. Alternatively or in addition, it is possible that the extent of free radical formation and disulfide bond reduction are directly related to the type and concentration of buffer components present in the crystal. Future work should systematically evaluate the effect of X-ray dose and dose rates and the impact of buffer components and their concentration on the extent to which disulfide bonds are X-ray damaged at room temperature.

S4. Assessing X-ray damage to functional active site residues at room temperature.

Functional active site residues that are often of most interest, in particular for enzymology studies in which cryo-structures and functional data are combined in structure-function analyses, have consistently been identified among the most susceptible to X-ray damage in cryo-cooled crystals (Adam *et al.*, 2009; Fioravanti *et al.*, 2007; Kort *et al.*, 2004; Matsui *et al.*, 2002; Sjöblom *et al.*, 2009; Taberman *et al.*, 2019; Weik *et al.*, 2000). While some of this tendency may result from more careful analysis of active sites, there is evidence that aspartate and glutamate residues, which are common at active sites, are more sensitive to X-ray damage than residues other than disulfide bonds (Burmeister, 2000; Fioravanti *et al.*, 2007; Ravelli & McSweeney, 2000; Weik *et al.*, 2000), including the lysozyme E35 and D52 active site residues previously described as highly-sensitive to damage (Weik *et al.*, 2000)

As little is known about the impact of X-ray damage on active site residues at room temperature, we evaluated the effects on lysozyme catalytic residues E35 and D52 and proteinase K catalytic residues D39, H69, and S224 (catalytic triad) and N161 (oxyanion hole). We focused on evaluating potential changes in

rotameric distributions. As above, we compared *Ringer* profiles and electron density maps from the least and most X-ray damaged RT datasets. These comparisons revealed nearly identical *Ringer* profiles with average $P_{CC} \geq 0.989 \pm 0.012$ (average and standard deviation, respectively) (**Figure S10A**), highly-similar 2Fo-Fc electron density maps, and featureless Fo-Fc and Fo-Fo difference electron density maps. The latter also indicated lack of major decarboxylation occurring due to X-ray damage (**Figure S10B-D**). In particular, while decarboxylation of acidic residues has been described as one of the most pervasive X-ray damage effects in cryo-cooled protein crystals (Burmeister, 2000; Fioravanti *et al.*, 2007), including the lysozyme E35 and D52 active site residues previously described as highly-sensitive to damage (Weik *et al.*, 2000), we found no evidence for significant X-ray damage to these active site residues in our RT data (**Figure S10**). Similarly, we observe no significant damage to the catalytic triad His 69 in proteinase K (**Figure S10**), in contrast to the high X-ray damage sensitivity observed for the equivalent His 440 in cryo-cooled crystals of acetylcholine esterase (Weik *et al.*, 2000). Our comparisons of the least and most X-ray damaged proteinase K and lysozyme RT datasets indicate lack of significant damage to functional active site residues and no changes in rotameric state populations (**Figure S10**), consistent with observations of lack of X-ray damage effects on the conformational distributions of functional active site residues in the enzyme CypA (Russi *et al.*, 2017). Thus, the results presented in this work extend previous findings and further increase the confidence in conformational heterogeneity information obtained from protein crystals at room temperature.

S5. Comparing X-ray damage effects on side chain rotameric distribution at cryo and room temperatures.

Figure S22 shows the overall distribution of temperature-induced rotameric changes identified from *Ringer* profiles with $P_{CC} \leq 0.95$ as obtained from comparison of the least X-ray damaged RT proteinase K dataset with the least (left) and the most X-ray damaged proteinase K cryo dataset (middle). While both comparisons point to structure-wide temperature-induced changes, the comparison with the more X-ray damaged cryo dataset shows nearly twice as many side chains that undergo apparent temperature-dependent conformational changes (43 vs 26, **Figures S19-S20**). Thus, X-ray damage under cryo conditions can lead to overestimates of temperature-induced changes, and these differences are observed throughout the structure (**Figure S22**).

S6. Modeling X-ray damage effects using B-factors.

With respect to modeling X-ray damage effects in cryo-cooled crystals, previous work suggested that the dominant X-ray damage effects could be adequately modelled by B-factors (Russi *et al.*, 2017). Our results indicate that while B-factors may generally provide adequate proxies for overall X-ray damage trends, in-

depth X-ray damage analyses benefits from more complex models that capture the appearance or disappearance of rotameric states, as B-factors do not adequately represent changes in rotameric states.

S7. X-ray damage effects and conformational heterogeneity at intermediate temperatures.

Global X-ray damage occurs at all temperatures, but the X-ray dose required to decrease the overall diffraction intensity (e.g. to halve the intensity) is much lower at cryo temperature (see *supplemental text* #2), allowing the collection of higher resolution data and/or more data. However, cryo-cooling can quench and alter conformational heterogeneity in cryo-cooled protein crystals relative to crystals at RT (Keedy, Kenner *et al.*, 2015; Lewandowski *et al.*, 2015; Ringe & Petsko, 2003; Tilton *et al.*, 1992). Thus, there are advantages and disadvantages associated with the collection of diffraction data from either cryo-cooled and RT crystals.

Recent work from multiple groups collectively suggested that collecting data at intermediate temperatures could have distinct advantages over data collected from either cryo-cooled or room temperatures crystals (Warkentin & Thorne, 2010). First, foundational work has provided evidence for activation of both harmonic and anharmonic motions in protein crystals above the protein glass transition temperature generally occurring within the 180-220 K temperature range (Ringe & Petsko, 2003; Tilton *et al.*, 1992). Building on this work, more recent studies provided evidence for a complex evolution of conformational heterogeneity in the 180-220 K temperature range, and also suggested that the vast majority of anharmonic motions, e.g., those responsible for the population of alternative side chain rotameric states, are activated at and above 250 K (Keedy, Kenner *et al.*, 2015; Lewandowski *et al.*, 2015). Thus, a body of work indicates that at 250 K, conformational heterogeneity should be similar to conformational heterogeneity at room temperature. Second, X-ray damage work by Warkentin and Thorne on thaumatin crystals indicated that at temperatures slightly below room temperature, crystals were more resistant to global X-ray damage than at RT (Warkentin & Thorne, 2010). They found that much of the increased resilience of protein crystals to global X-ray damage observed at 100 K relative to RT can be achieved by cooling the crystals to temperatures below RT but above the protein glass transition where solvent remains fluid (Warkentin & Thorne, 2010). Thus, prior work indicates that, while conformational heterogeneity in protein crystals is expected to be similar at 250 K and room temperature, more diffraction data can be collected at 250 K relative to RT from a given protein crystal, making 250 K a temperature of particular interest for protein X-ray crystallography.

Because X-ray damage has pervasive effects on protein structure at cryo temperatures, including alteration of conformational heterogeneity, while X-ray damage effects appear minimal at room temperature, it is currently unclear how X-ray damage would affect conformational heterogeneity at 250 K. Thus, to

confidently model conformational heterogeneity using diffraction data collected at 250 K, there is a need to evaluate the effects of X-ray damage at this intermediate temperature.

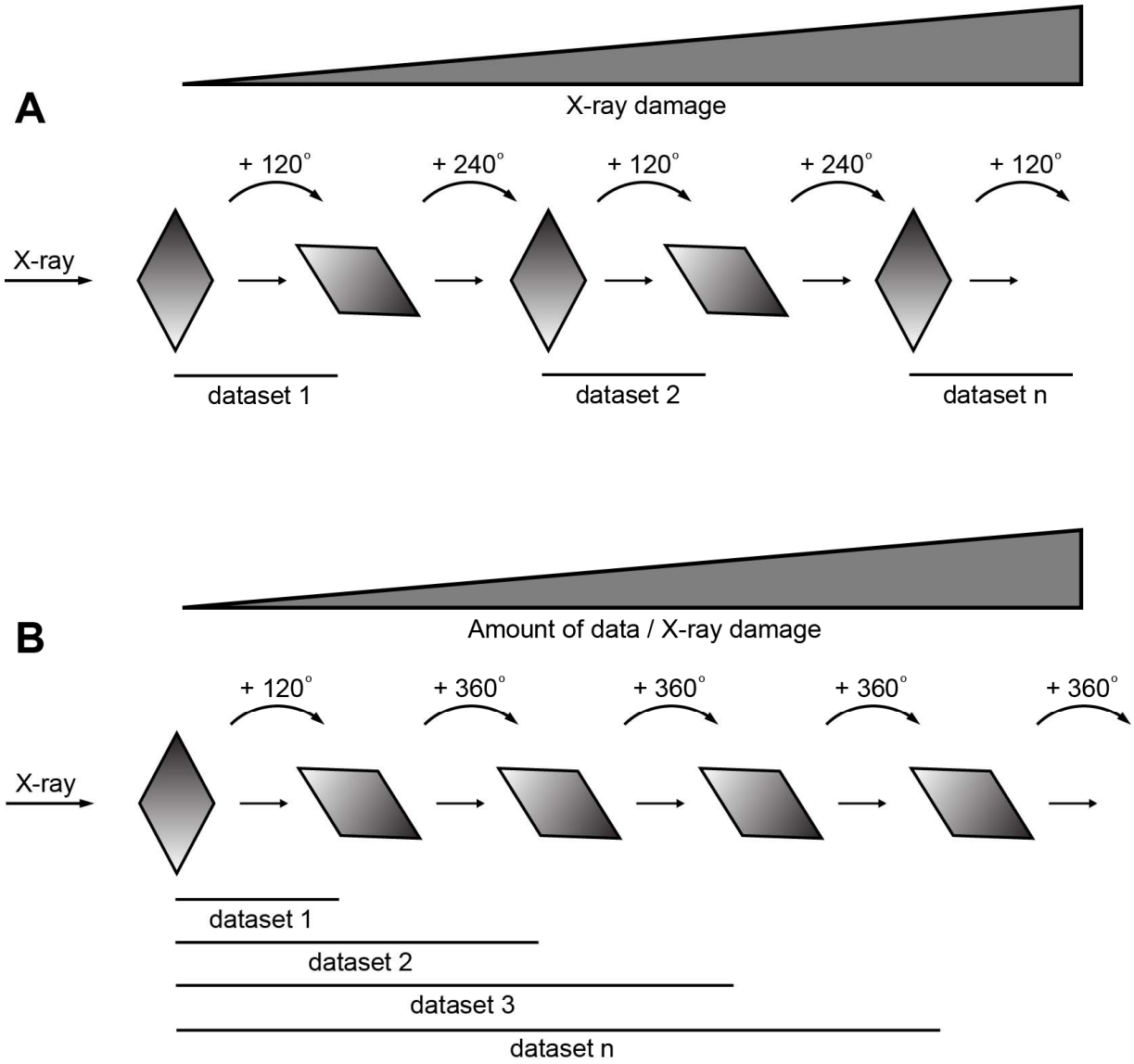

Figure S1 X-ray diffraction dataset collection. Increasingly X-ray damaged diffraction data from proteinase K, thaumatin, and lysozyme protein crystals were collected using the traditional oscillation approach in which diffraction data are collected while the crystal is being rotated around the goniometer axis (Dauter, 2017, 1999). The increasingly X-ray damaged data can be grouped in (A) datasets collected from the same crystal orientation and containing the same amount of diffraction data to ensure that the only experimental variable is the extent of X-ray damage (referred to herein as "sequential" X-ray damaged datasets) or (B) in merged X-ray datasets in which increasingly X-ray damaged data are merged together, as done in typical diffraction data collection for structural studies (referred to herein as "cumulative" X-ray damaged datasets).

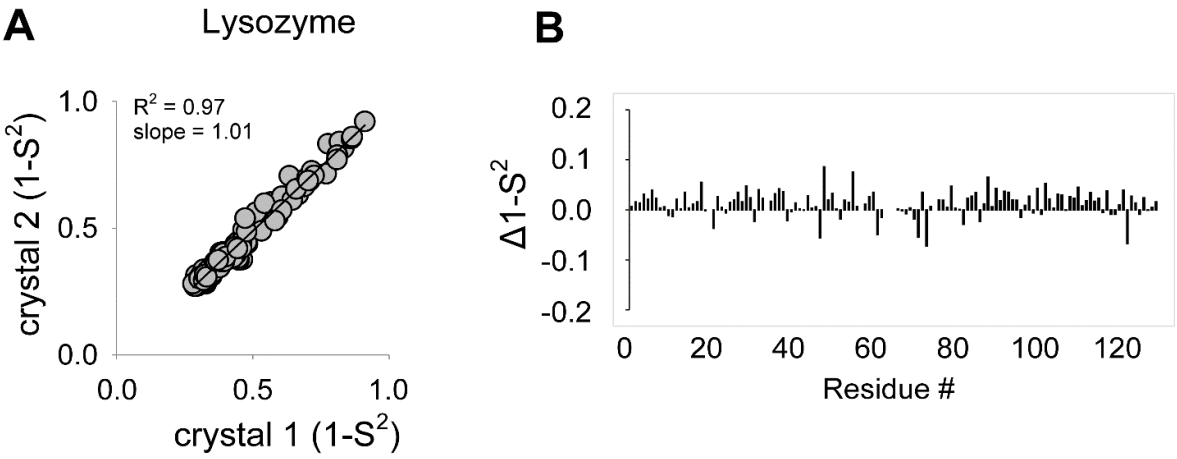

Figure S2 Comparison of (1-S^2) values from two independent lysozyme crystals at room temperature indicates highly similar conformational heterogeneity. (A) Correlation plot and (B) difference (1-S^2) as a function of residue number.

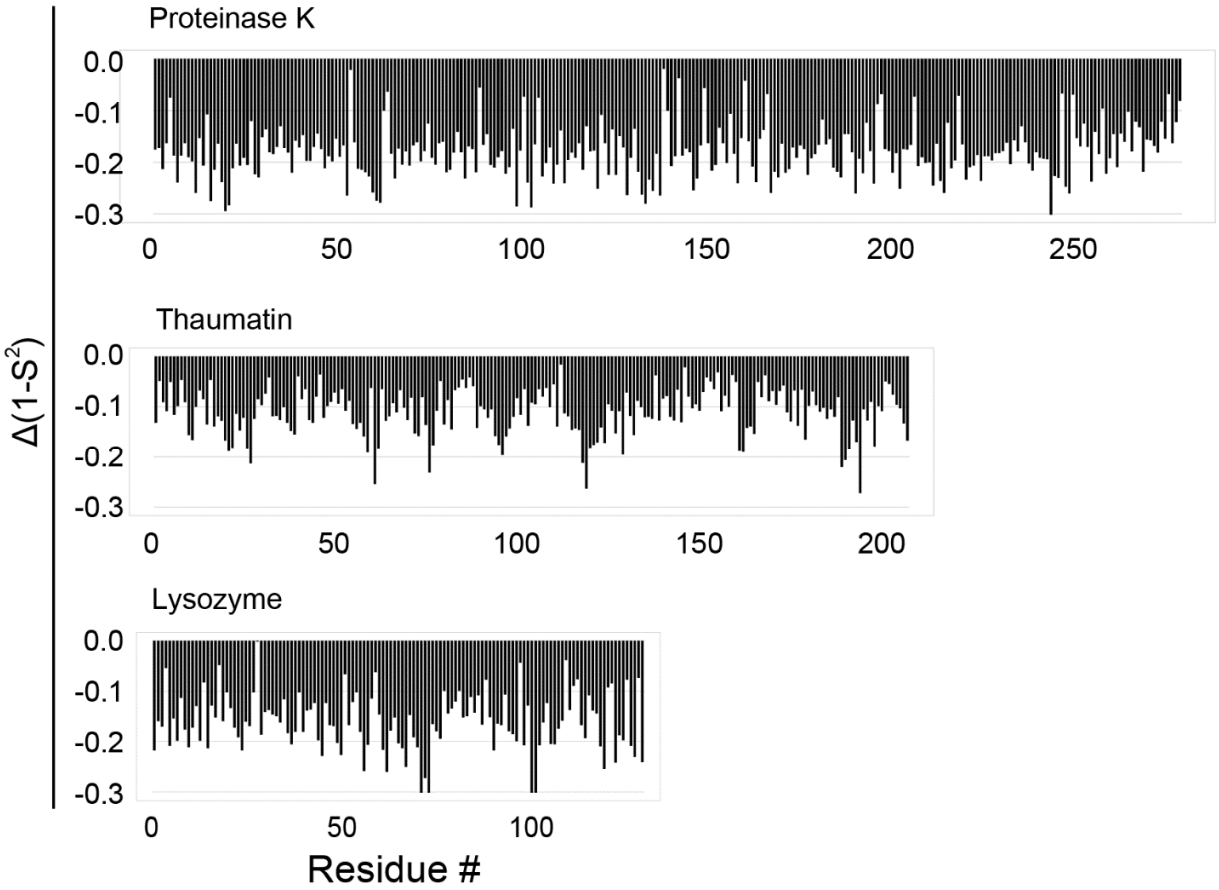

Figure S3 X-ray damage leads to a modest but measurable increase in conformational heterogeneity as captured by disorder parameters ($1-S^2$) in protein crystals at room temperature. $\Delta(1-S^2)$ values between the least and most damaged room temperature datasets for proteinase K, thaumatin, and lysozyme were obtained by subtracting the most damaged from the least damaged ($1-S^2$) values for each residue; the negative ($1-S^2$) values thus indicate higher ($1-S^2$) values obtained from the most damaged dataset. The increased ($1-S^2$) values in the most damaged dataset are not due to resolution differences (see **Figure S5**).

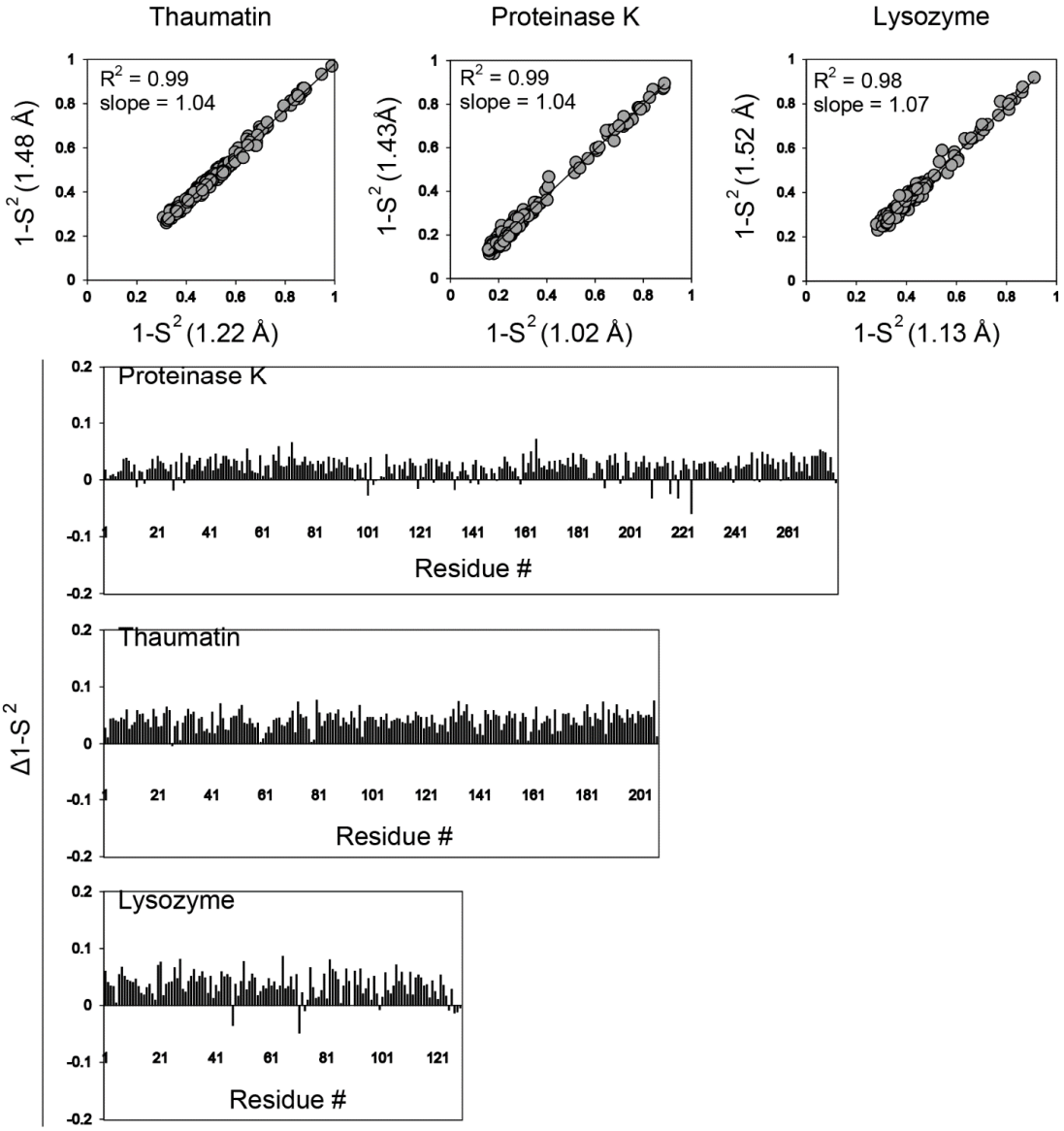

Figure S4 Decreasing resolution does not lead to major changes in the calculated ($1\text{-}S^2$) values. Comparison of ($1\text{-}S^2$) values from the multi-conformer models obtained from the least damaged dataset when the dataset is of optimal resolution (1.02 Å, 1.22 Å and 1.13 Å for proteinase K, thaumatin, and lysozyme, respectively) and when the resolution of the same dataset is cut to match the resolution of the most damaged dataset (1.43 Å, 1.48 Å, and 1.52 Å for proteinase K, thaumatin, and lysozyme, respectively; see Materials and Methods). Correlation plots (top) and difference ($1\text{-}S^2$) (bottom) as a function of residue number. The analysis indicates that the lower resolution of the most damaged datasets does not appear as a main factor contributing to the observed increase in ($1\text{-}S^2$) values with X-ray damage in Figure S7. The $\Delta(1\text{-}S^2)$ are small and positive in contrast to the larger negative $\Delta(1\text{-}S^2)$ observed in Figure S7.

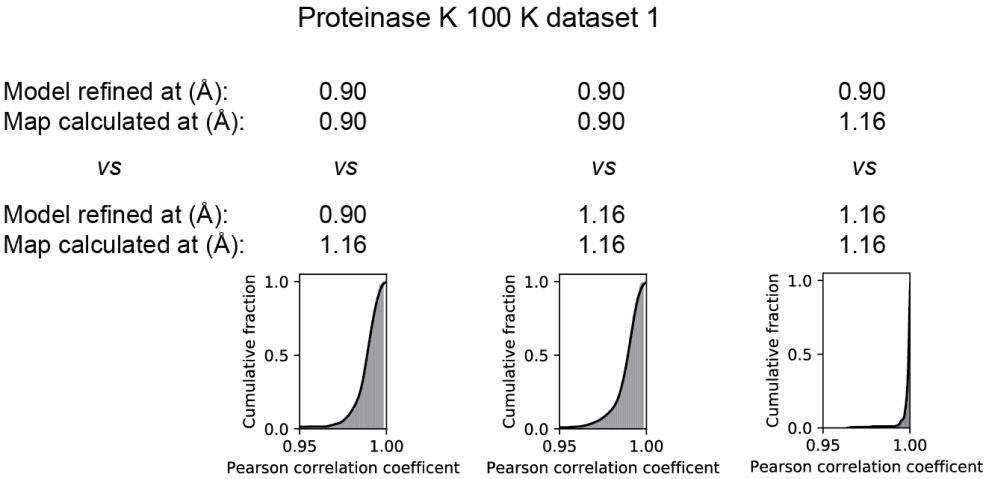

Figure S5 Matching electron density map resolution is required for accurate *Ringer* analysis and Pearson correlation coefficients calculation. The resolution of diffraction datasets inevitably decreases with increasing X-ray damage. Thus, for all protein crystals in this work, the least X-ray damaged and increasingly (most) damaged datasets are of different resolutions, with the least damaged dataset being of highest resolution. To evaluate the effect of electron density map resolution on calculating Pearson correlation coefficients (P_{CC}) from *Ringer* plots, we compared the *Ringer* profiles obtained from the least damaged proteinase K dataset which was either refined at the optimal resolution of the dataset (0.90 Å) or at a reduced resolution (1.16 Å) to match the resolution of the most damaged dataset and the electron density map used for obtaining *Ringer* plots was either left at the optimal resolution (0.90 Å) or reduced to match the resolution of the most damaged dataset (1.16 Å). Thus, *Ringer* profiles were obtained from three possible combinations of resolutions used for refinement and resolutions used for map calculations: 0.90 Å and 0.90 Å, 0.90 Å and 1.16 Å, and 1.16 Å and 1.16 Å, respectively. The fourth possible combination of 1.16 Å (refinement) and 0.90 Å (map calculation) was not included as this scenario is not relevant for the analysis. The analysis shows that for the same least damaged dataset, artifactually lower P_{CC} values are obtained if the resolutions of the electron density maps used for calculating *Ringer* profiles do not match (left and middle plots of cumulative fraction P_{CC}). The plot of cumulative fraction P_{CC} on the right shows that when the resolution of the electron density maps is matched (i.e. 1.16 Å) there is a near perfect agreement between the *Ringer* profiles (P_{CC} is close to 1.0) with small differences originating from small coordinate changes due to the same model being refined against two different resolution datasets. Thus, all *Ringer* comparisons between increasingly damaged datasets have been performed by calculating *Ringer* profiles from electron density maps with matched resolutions –e.g., the for the comparison of the least and most damaged proteinase K cryo datasets, each structural model has been refined at the optimal dataset resolution (0.90 Å and 1.16 Å, respectively) but the *Ringer* profiles were calculated using electron density maps at 1.16 Å.

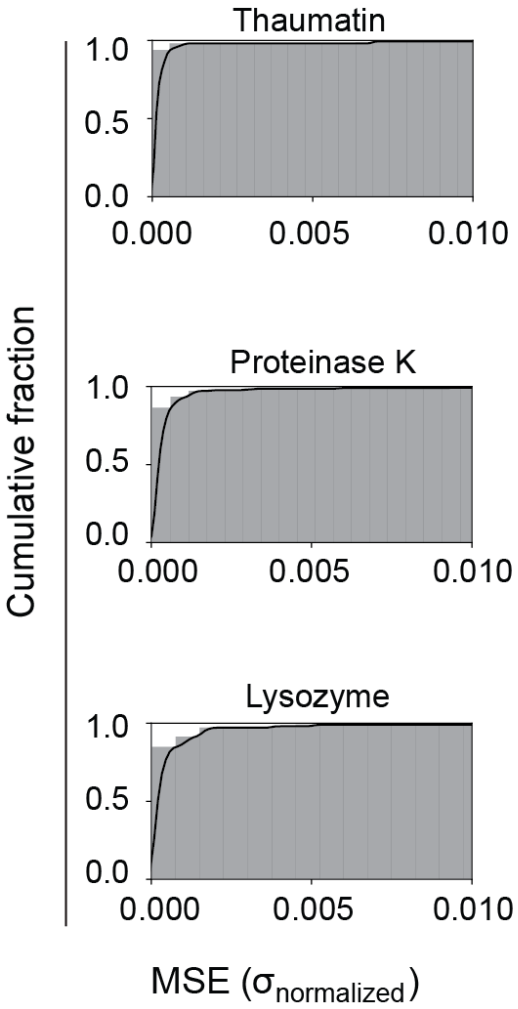

Figure S6 Modest effects of X-ray damage on side-chain rotameric distributions at room temperature. Mean square errors (MSE) were obtained in the same way as Pearson correlation coefficients (PCC) in Figure 3A except that MSEs represent the agreement between the experimental correlation and a slope = 1 correlation line (diagonal) from correlation plots between electron density values (σ) of two datasets, each plotted on x-axis and y-axis as illustrated in Figures 3. The cumulative fractions of MSEs shown here are from correlation plots between electron density values (σ) of the least damaged (x-axis) and most damaged (y-axis) datasets for the dihedral angle χ1 of each residue in thaumatin (top), proteinase K (middle), and lysozyme (bottom).

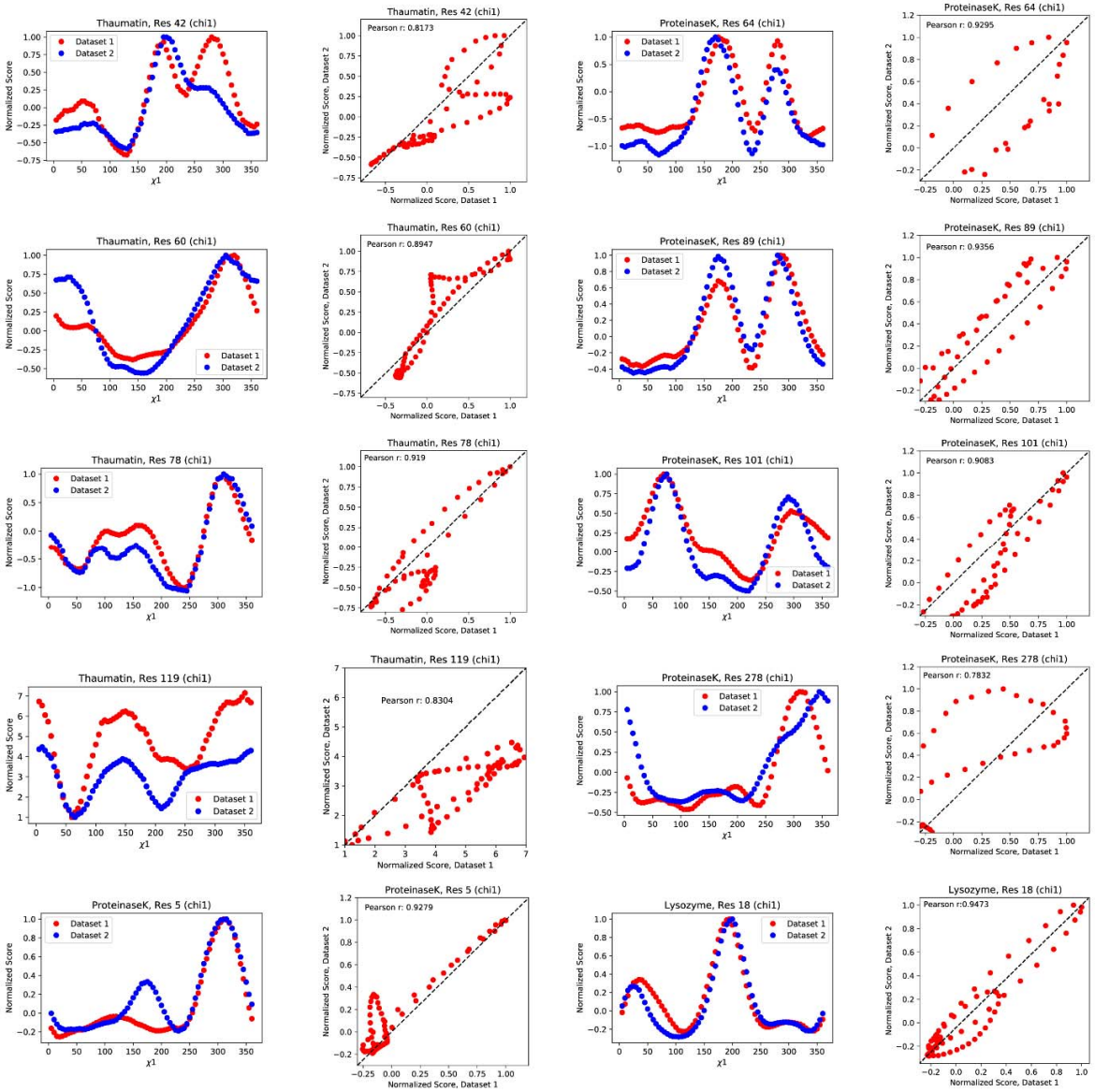

Figure S7 X-ray damage does not lead to major changes in side chain rotameric states in protein crystals at room temperature. Normalized *Ringer* profiles of the least (red) and most (blue) damaged datasets for thaumatin, proteinase K, and lysozyme for all residues with Pearson correlation coefficients (P_{CC}) ≤ 0.95 and the associated correlation plots and respective P_{CC} values.

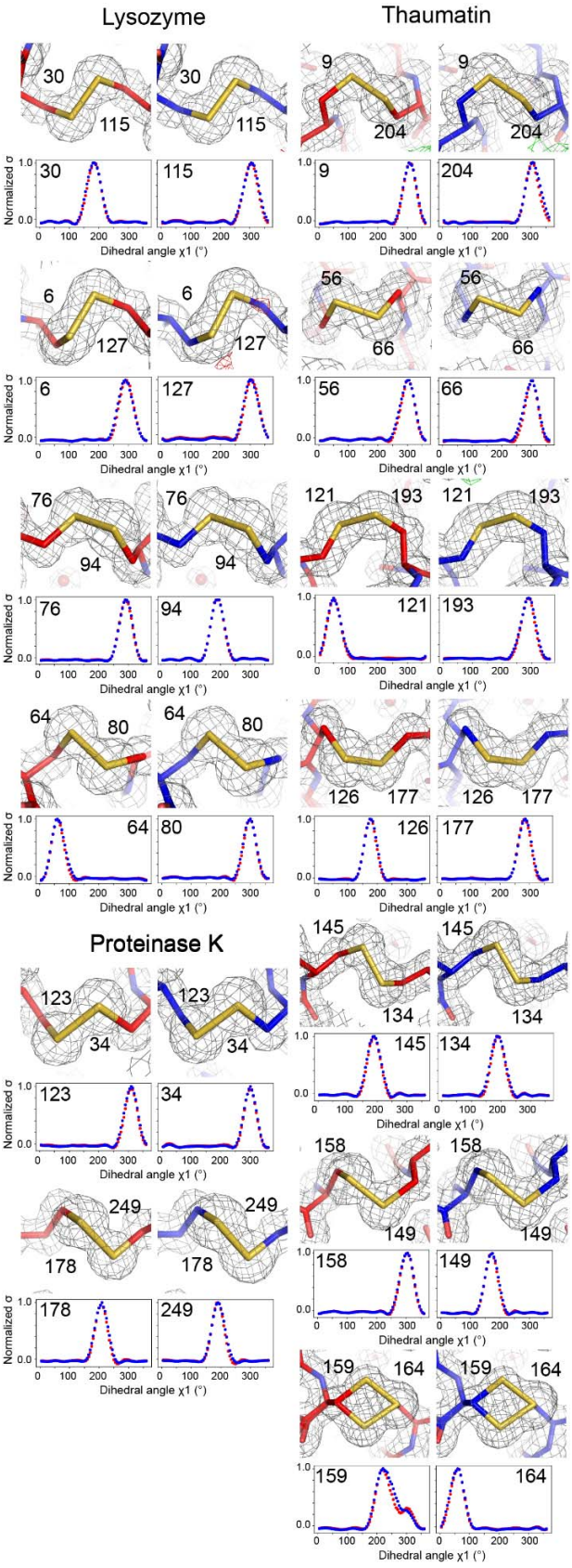
Lysozyme
Thaumatin
Proteinase K
Normalized σ
Dihedral angle χ1 (°)

Figure S8 *Ringer* and electron density analyses indicate limited X-ray damage to disulfide bonds at room temperature. Electron density maps (2Fo-Fc in grey mesh at a contour level of 1σ, negative and positive Fo-Fc peaks in red and green mesh, respectively, at a contour level of 3σ) and refined structural models (shown in sticks) for the least damaged (red) and most damaged (blue) datasets for lysozyme, proteinase K, and thaumatin (Tables S1-S3). The normalized *Ringer* profiles were obtained for each cysteine residue from the least damaged dataset (red) and most damaged dataset (blue) for each protein and PCC were calculated as described in Materials and Methods.

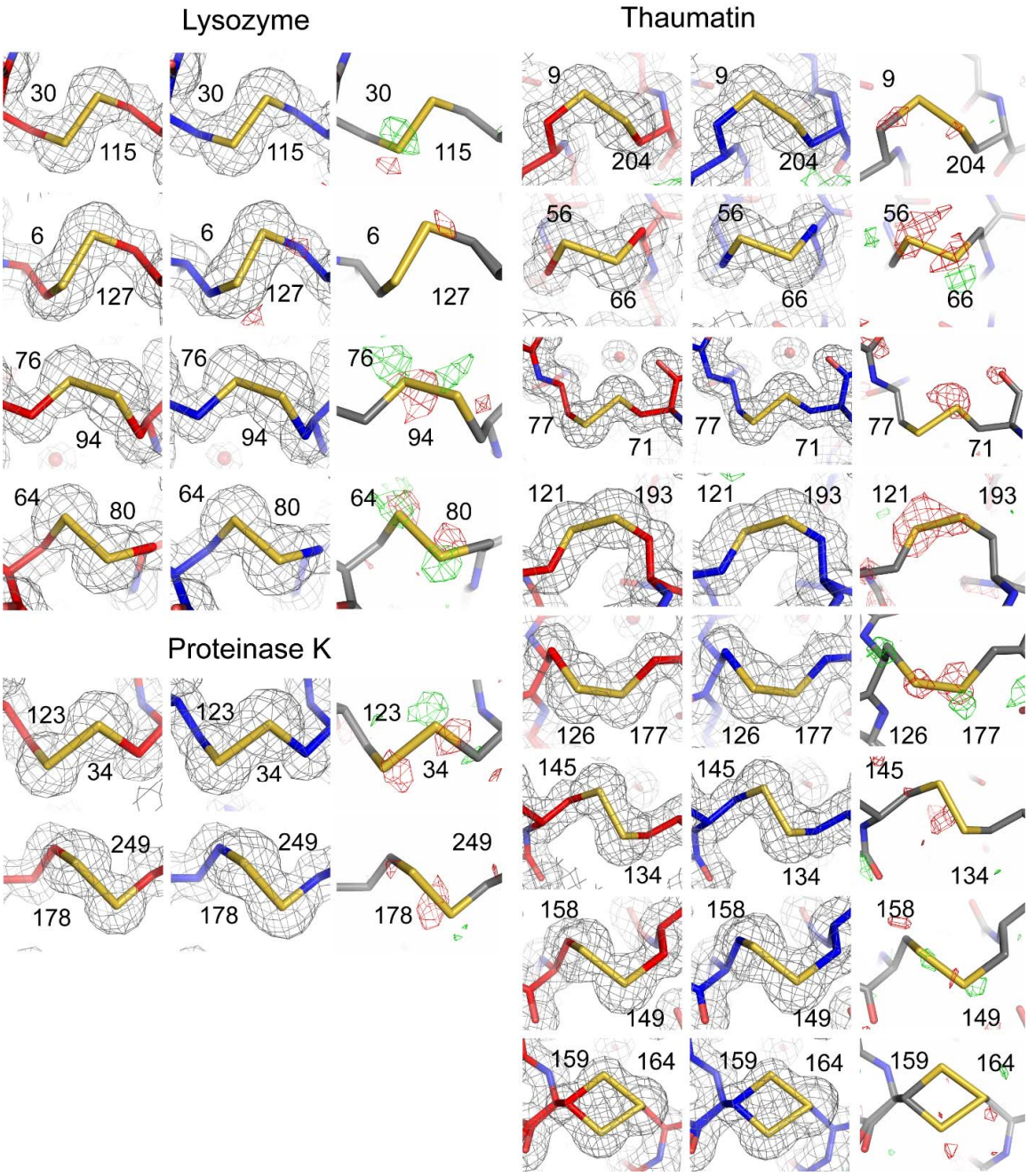

Figure S9 Difference electron density (Fo-Fo) maps provide evidence for limited X-ray damage to disulfide bonds at room temperature. Shown are the refined structural models (shown in sticks) for the least damaged (red) and most damaged (blue) datasets for lysozyme, proteinase K, and thaumatin, the associated electron density maps (2Fo-Fc, grey mesh at 1σ, left and middle), and difference electron density maps (Fo-Fo, negative and positive peaks in red and green mesh, respectively, at a contour level of 3σ, right).

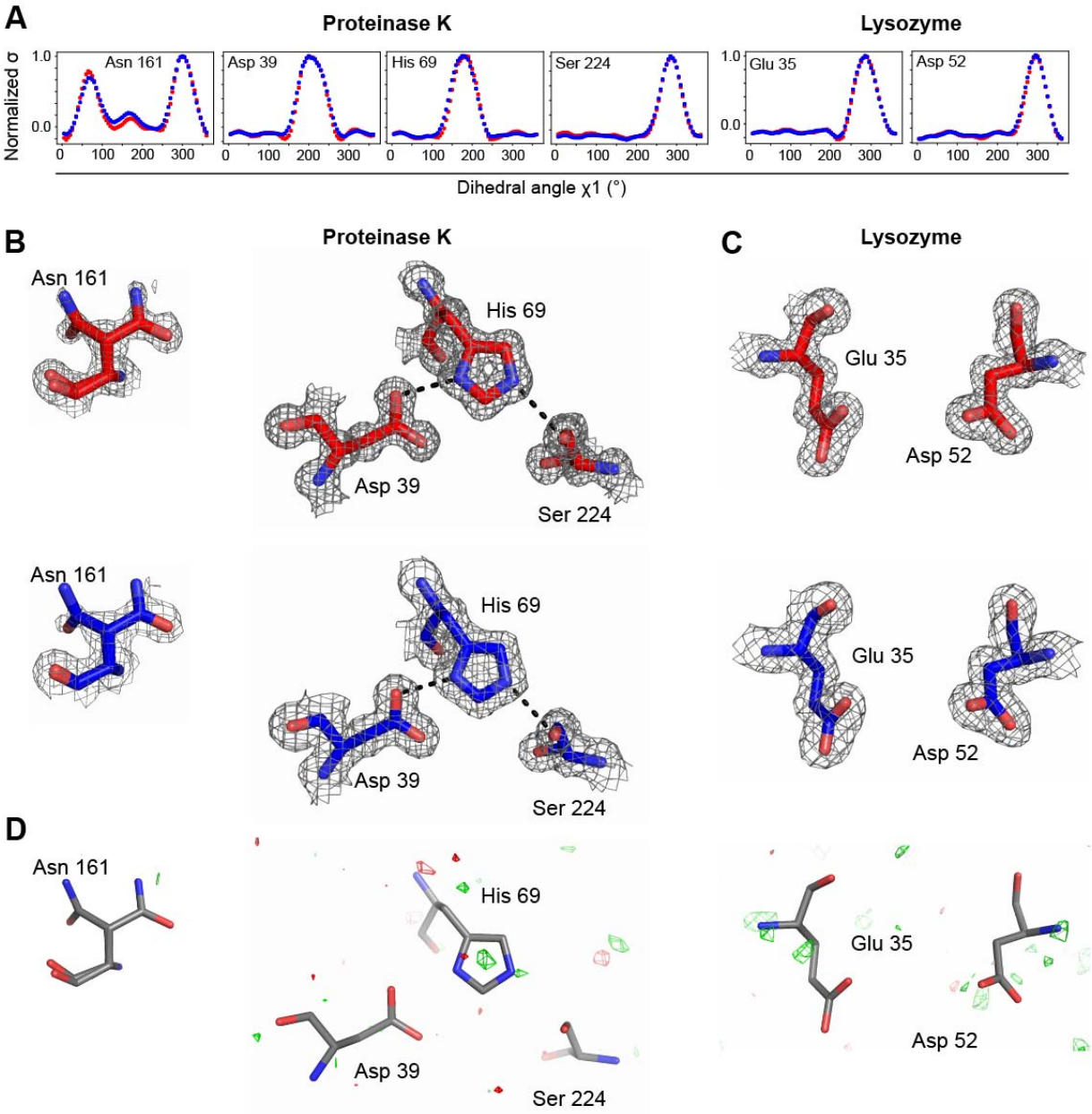

Figure S10 Absence of substantial X-ray damage to active site residues at room temperature. (A) Normalized *Ringer* profiles for dihedral angles χ1 obtained from the least and most damaged datasets (red and blue, respectively). (B) Electron density and stick models for the proteinase K oxyanion hole hydrogen bond donor N161 and catalytic triad S224, H69, and D39 and (C) the lysozyme catalytic residues E35 and D52. (B, C) The electron density map (2Fo-Fc in grey mesh at a contour level of 1σ) and refined structural models (sown in sticks) for the least damaged (red) and most damaged (blue) datasets for each protein. (D) The Fo-Fo difference electron density maps between the least and most damaged datasets contoured at 3σ (positive peaks in green mesh and negative peaks in red mesh) for proteinase K and lysozyme active site residues shown above in panels B and C.

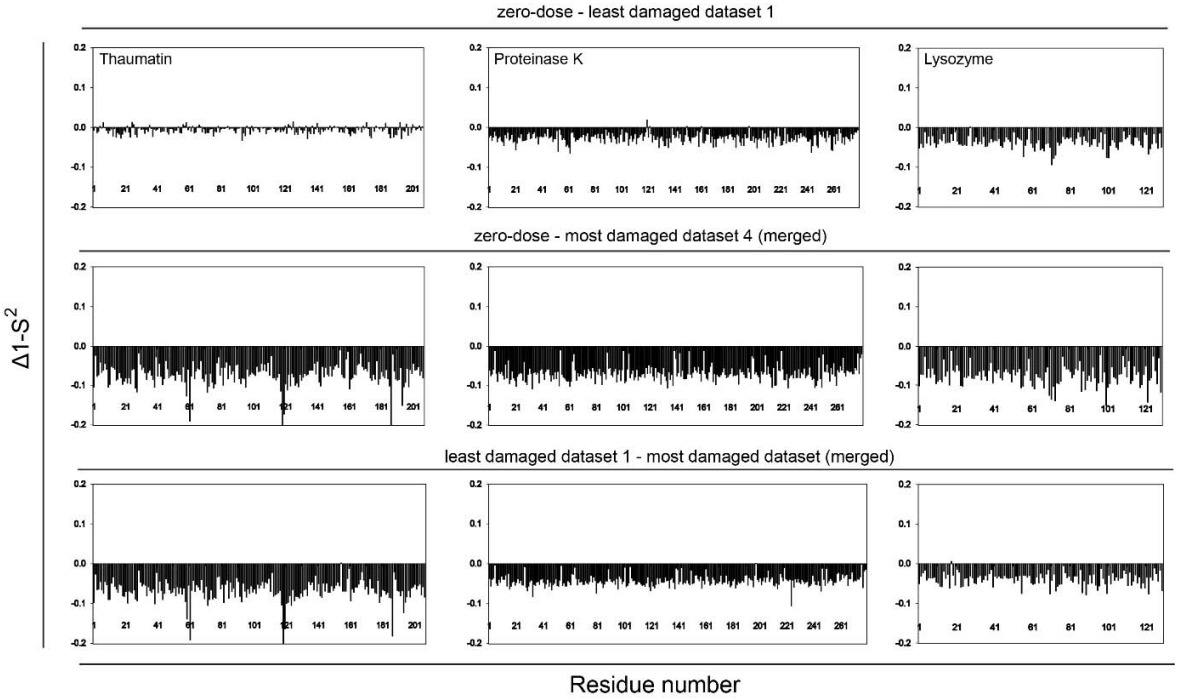

Figure S11 Comparison of the (1-S^2) values obtained from the least damaged and most damaged (merged) room temperature datasets and the (1-S^2) values extrapolated to zero-dose. The figure shows Δ(1-S^2) values between extrapolated zero-dose (1-S^2) and least damaged (1-S^2) (top), extrapolated zero-dose (1-S^2) and most damaged (merged) (1-S^2) (middle), and least damaged (1-S^2) and most damaged (merged) (bottom). Overall, the lowest Δ(1-S^2) values are between the zero-dose (1-S^2) and least damaged (1-S^2), providing confidence in using (1-S^2) values for functional analyses if zero-dose (1-S^2) values cannot be obtained.

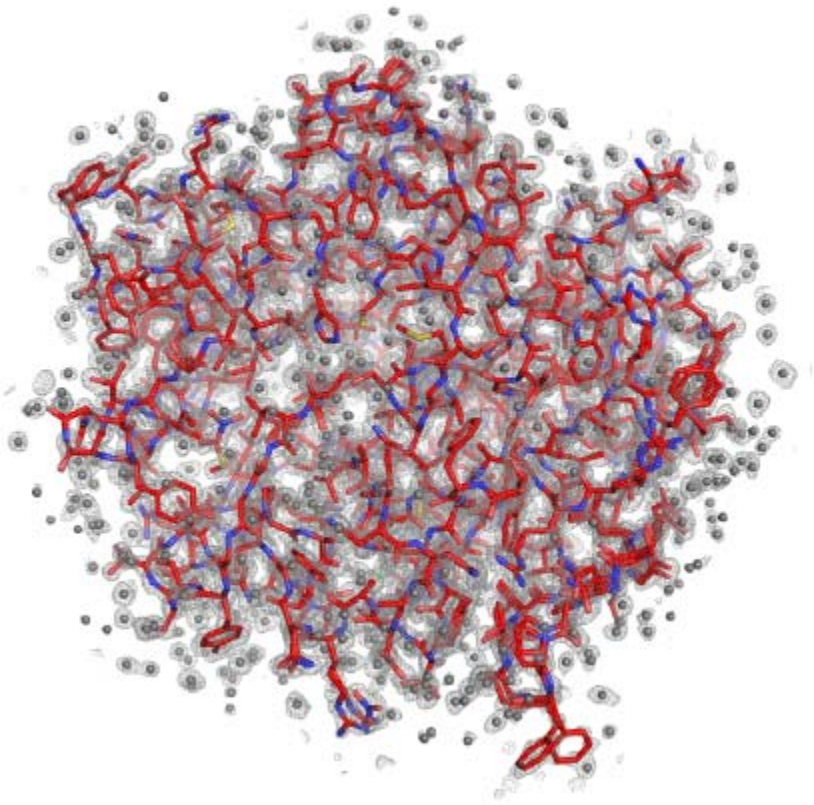

Figure S12 100 K structural model of proteinase K (red sticks) and its electron density map (grey mesh, final 2Fo-Fc electron density map contoured at 1σ) refined using the least damaged dataset (dataset 1, see Table S11). Water molecules are shown as grey spheres

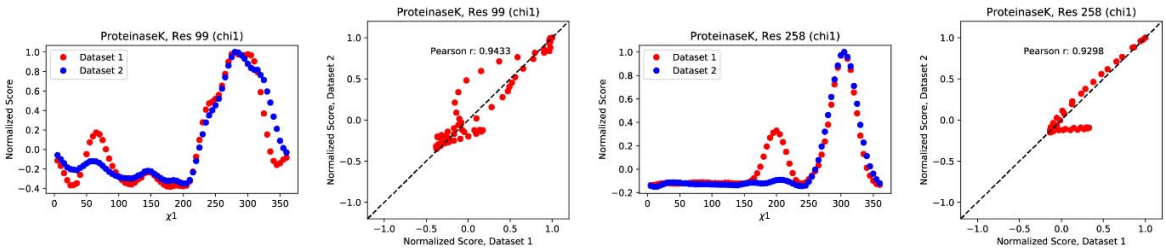

Figure S13 Normalized *Ringer* profiles with Pearson correlation coefficients (PCC) $\leq$ 0.95 from proteinase K 100 K data for dataset 1 (red) and dataset 2 (blue). Also shown are the associated correlation plots and respective PCC values.

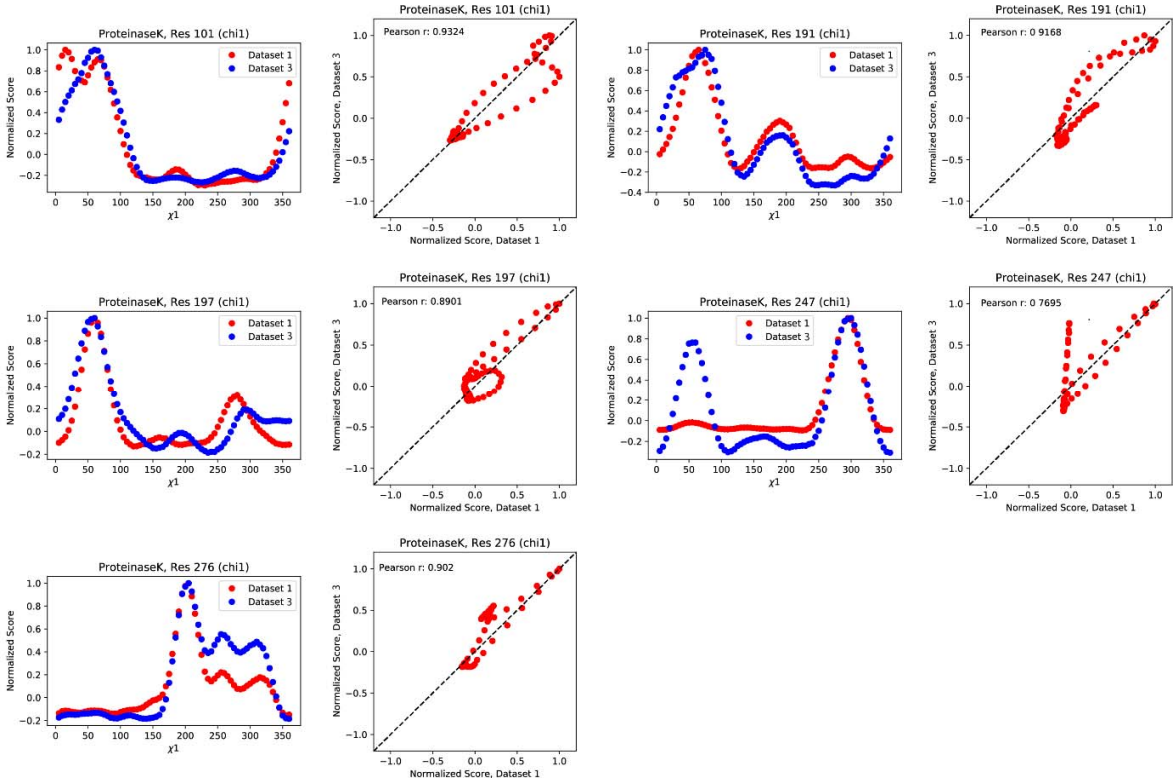

Figure S14 Normalized *Ringer* profiles with Pearson correlation coefficients (PCC) ≤ 0.95 from proteinase K 100 K data for dataset 1 (red) and dataset 3 (blue). Also shown are the associated correlation plots and respective PCC values.

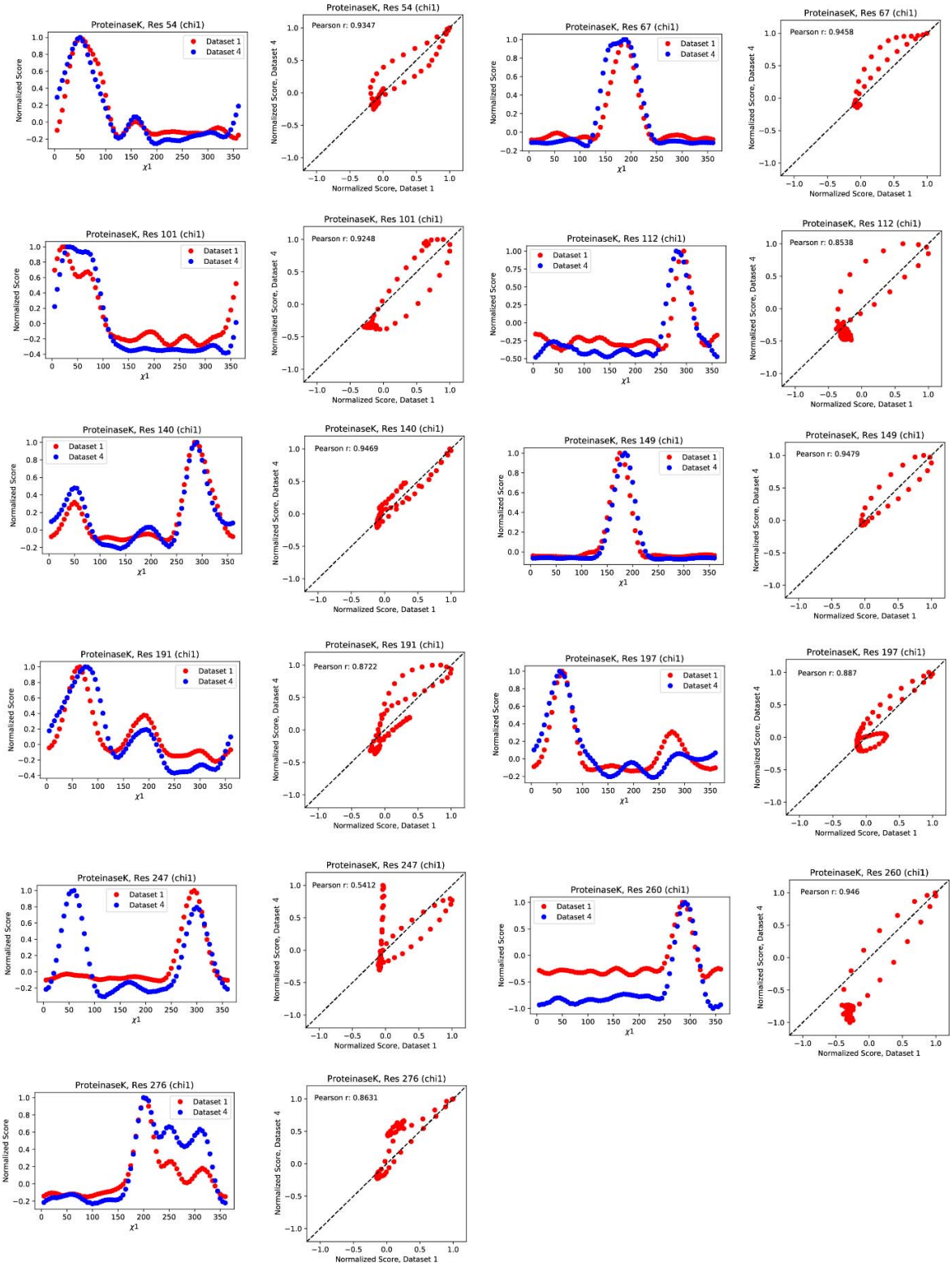
ProteinaseK, Res 54 (chi1)
Dataset 1
Dataset 4
Normalized Score
χ1
ProteinaseK, Res 54 (chi1)
Pearson r: 0.9347
Normalized Score, Dataset 4
Normalized Score, Dataset 1
ProteinaseK, Res 67 (chi1)
Dataset 1
Dataset 4
Normalized Score
χ1
ProteinaseK, Res 67 (chi1)
Pearson r: 0.9458
Normalized Score, Dataset 4
Normalized Score, Dataset 1
ProteinaseK, Res 101 (chi1)
Dataset 1
Dataset 4
Normalized Score
χ1
ProteinaseK, Res 101 (chi1)
Pearson r: 0.9248
Normalized Score, Dataset 4
Normalized Score, Dataset 1
ProteinaseK, Res 112 (chi1)
Dataset 1
Dataset 4
Normalized Score
χ1
ProteinaseK, Res 112 (chi1)
Pearson r: 0.8538
Normalized Score, Dataset 4
Normalized Score, Dataset 1
ProteinaseK, Res 140 (chi1)
Dataset 1
Dataset 4
Normalized Score
χ1
ProteinaseK, Res 140 (chi1)
Pearson r: 0.9469
Normalized Score, Dataset 4
Normalized Score, Dataset 1
ProteinaseK, Res 149 (chi1)
Dataset 1
Dataset 4
Normalized Score
χ1
ProteinaseK, Res 149 (chi1)
Pearson r: 0.9479
Normalized Score, Dataset 4
Normalized Score, Dataset 1
ProteinaseK, Res 191 (chi1)
Dataset 1
Dataset 4
Normalized Score
χ1
ProteinaseK, Res 191 (chi1)
Pearson r: 0.8722
Normalized Score, Dataset 4
Normalized Score, Dataset 1
ProteinaseK, Res 197 (chi1)
Dataset 1
Dataset 4
Normalized Score
χ1
ProteinaseK, Res 197 (chi1)
Pearson r: 0.887
Normalized Score, Dataset 4
Normalized Score, Dataset 1
ProteinaseK, Res 247 (chi1)
Dataset 1
Dataset 4
Normalized Score
χ1
ProteinaseK, Res 247 (chi1)
Pearson r: 0.5412
Normalized Score, Dataset 4
Normalized Score, Dataset 1
ProteinaseK, Res 260 (chi1)
Dataset 1
Dataset 4
Normalized Score
χ1
ProteinaseK, Res 260 (chi1)
Pearson r: 0.946
Normalized Score, Dataset 4
Normalized Score, Dataset 1
ProteinaseK, Res 276 (chi1)
Dataset 1
Dataset 4
Normalized Score
χ1
ProteinaseK, Res 276 (chi1)
Pearson r: 0.8631
Normalized Score, Dataset 4
Normalized Score, Dataset 1

Figure S15 Normalized *Ringer* profiles with Pearson correlation coefficients (PCC) ≤ 0.95 from proteinase K 100 K data for dataset 1 (red) and dataset 4 (blue). Also shown are the associated correlation plots and respective PCC values.

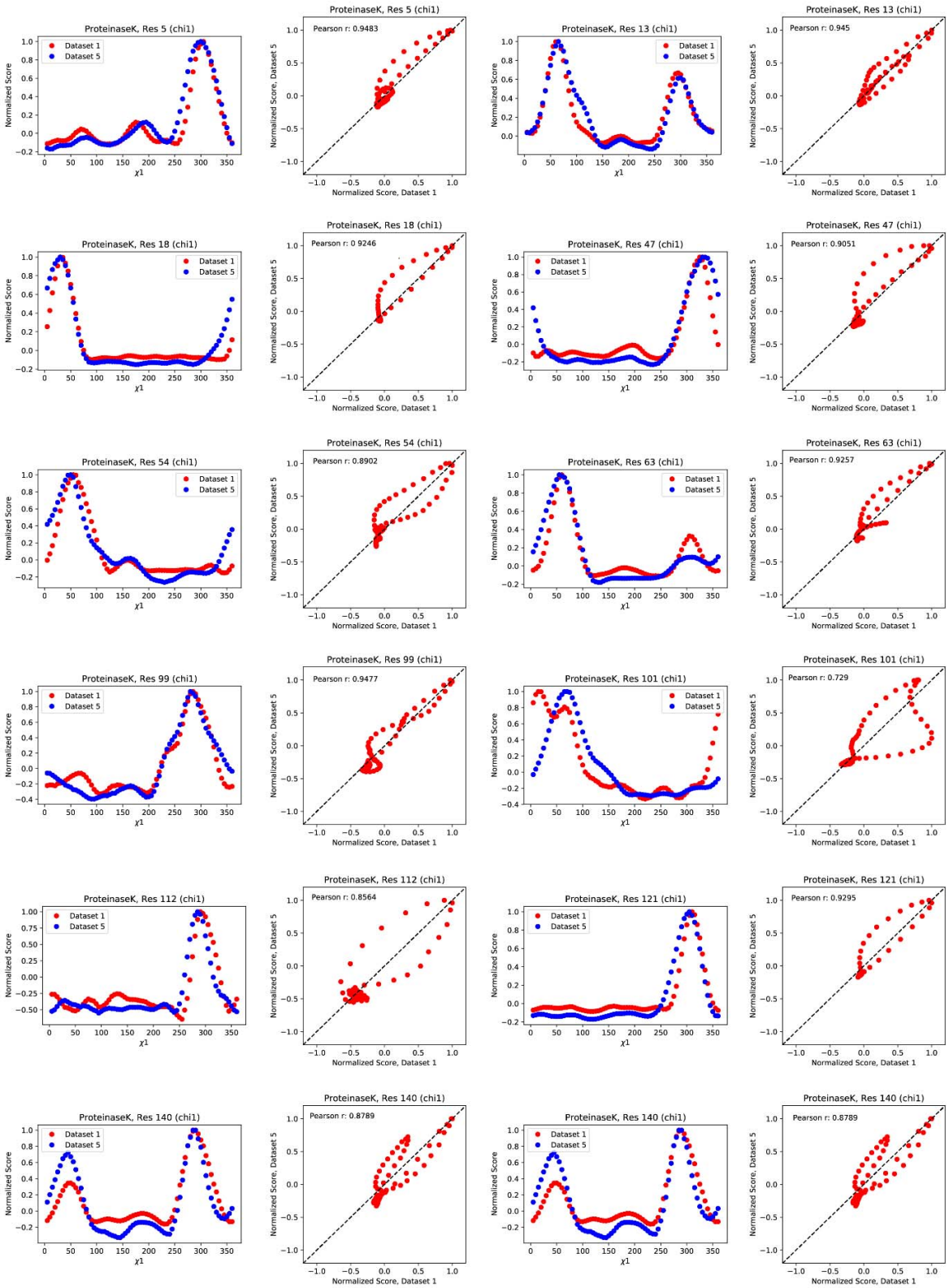
ProteinaseK, Res 5 (chi1)
Dataset 1
Dataset 5
Normalized Score
χ1
ProteinaseK, Res 5 (chi1)
Pearson r: 0.9483
Normalized Score, Dataset 5
Normalized Score, Dataset 1
ProteinaseK, Res 13 (chi1)
Dataset 1
Dataset 5
Normalized Score
χ1
ProteinaseK, Res 13 (chi1)
Pearson r: 0.945
Normalized Score, Dataset 5
Normalized Score, Dataset 1
ProteinaseK, Res 18 (chi1)
Dataset 1
Dataset 5
Normalized Score
χ1
ProteinaseK, Res 18 (chi1)
Pearson r: 0 9246
Normalized Score, Dataset 5
Normalized Score, Dataset 1
ProteinaseK, Res 47 (chi1)
Dataset 1
Dataset 5
Normalized Score
χ1
ProteinaseK, Res 47 (chi1)
Pearson r: 0.9051
Normalized Score, Dataset 5
Normalized Score, Dataset 1
ProteinaseK, Res 54 (chi1)
Dataset 1
Dataset 5
Normalized Score
χ1
ProteinaseK, Res 54 (chi1)
Pearson r: 0.8902
Normalized Score, Dataset 5
Normalized Score, Dataset 1
ProteinaseK, Res 63 (chi1)
Dataset 1
Dataset 5
Normalized Score
χ1
ProteinaseK, Res 63 (chi1)
Pearson r: 0.9257
Normalized Score, Dataset 5
Normalized Score, Dataset 1
ProteinaseK, Res 99 (chi1)
Dataset 1
Dataset 5
Normalized Score
χ1
ProteinaseK, Res 99 (chi1)
Pearson r: 0.9477
Normalized Score, Dataset 5
Normalized Score, Dataset 1
ProteinaseK, Res 101 (chi1)
Dataset 1
Dataset 5
Normalized Score
χ1
ProteinaseK, Res 101 (chi1)
Pearson r: 0.729
Normalized Score, Dataset 5
Normalized Score, Dataset 1
ProteinaseK, Res 112 (chi1)
Dataset 1
Dataset 5
Normalized Score
χ1
ProteinaseK, Res 112 (chi1)
Pearson r: 0.8564
Normalized Score, Dataset 5
Normalized Score, Dataset 1
ProteinaseK, Res 121 (chi1)
Dataset 1
Dataset 5
Normalized Score
χ1
ProteinaseK, Res 121 (chi1)
Pearson r: 0.9295
Normalized Score, Dataset 5
Normalized Score, Dataset 1
ProteinaseK, Res 140 (chi1)
Dataset 1
Dataset 5
Normalized Score
χ1
ProteinaseK, Res 140 (chi1)
Pearson r: 0.8789
Normalized Score, Dataset 5
Normalized Score, Dataset 1
ProteinaseK, Res 140 (chi1)
Dataset 1
Dataset 5
Normalized Score
χ1
ProteinaseK, Res 140 (chi1)
Pearson r: 0.8789
Normalized Score, Dataset 5
Normalized Score, Dataset 1

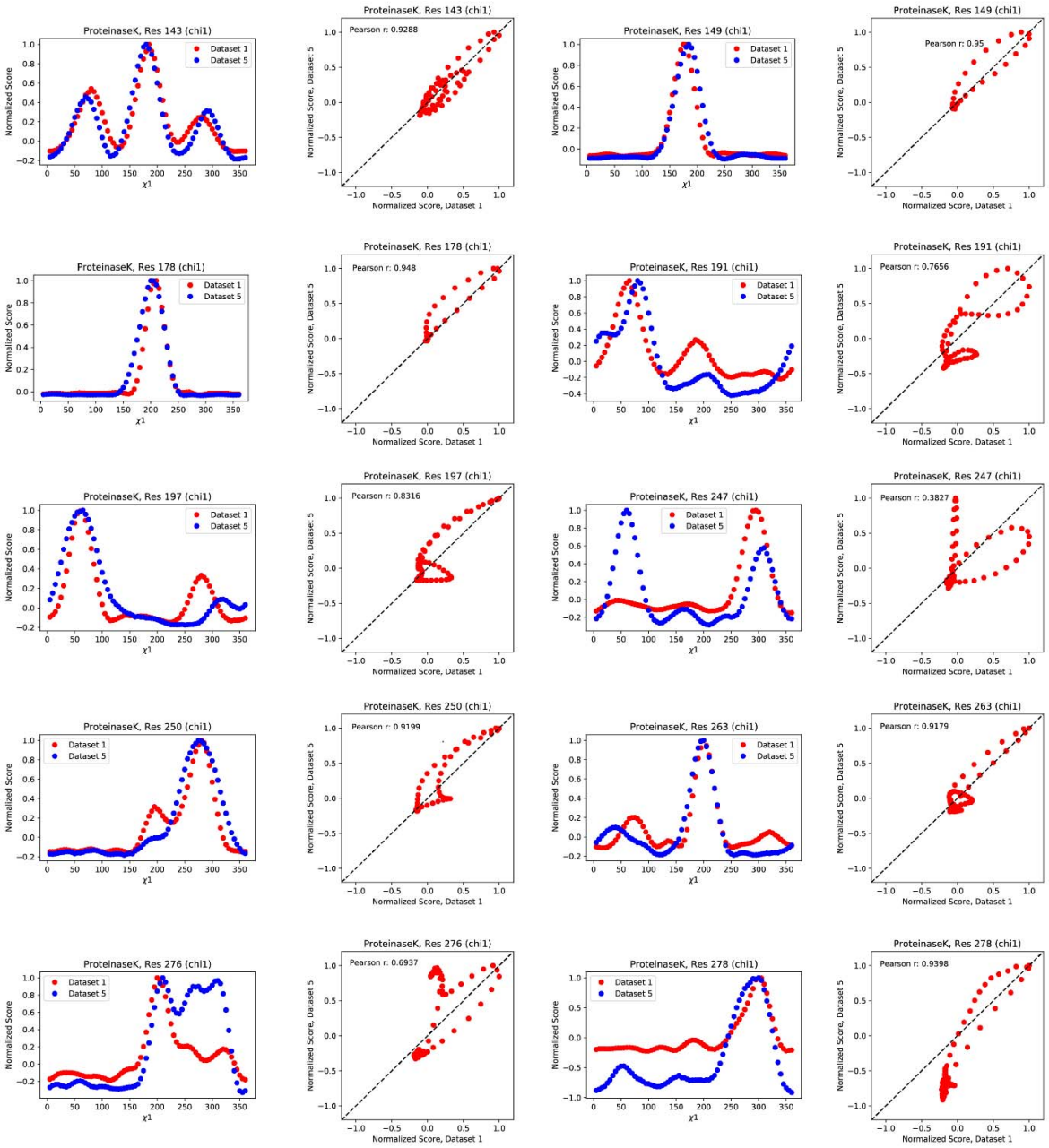

Figure S16 Normalized *Ringer* profiles with Pearson correlation coefficients (P_{CC}) ≤ 0.95 from proteinase K 100 K data for dataset 1 (red) and dataset 5 (blue). Also shown are the associated correlation plots and respective P_{CC} values.

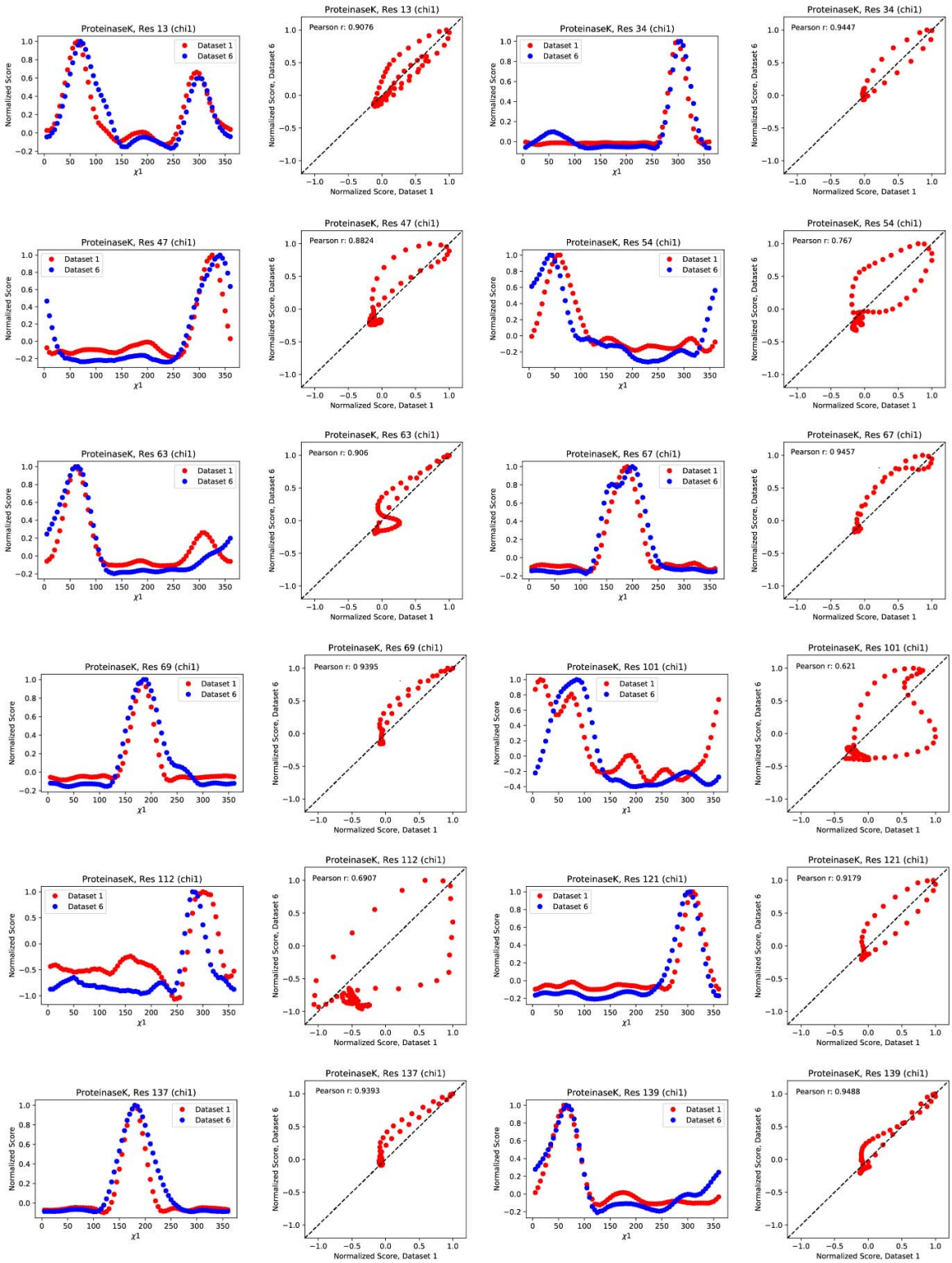
ProteinaseK, Res 13 (chi1)
Dataset 1
Dataset 6
Normalized Score
χ1
ProteinaseK, Res 13 (chi1)
Pearson r: 0.9076
Normalized Score, Dataset 6
Normalized Score, Dataset 1
ProteinaseK, Res 34 (chi1)
Dataset 1
Dataset 6
Normalized Score
χ1
ProteinaseK, Res 34 (chi1)
Pearson r: 0.9447
Normalized Score, Dataset 6
Normalized Score, Dataset 1
ProteinaseK, Res 47 (chi1)
Dataset 1
Dataset 6
Normalized Score
χ1
ProteinaseK, Res 47 (chi1)
Pearson r: 0.8824
Normalized Score, Dataset 6
Normalized Score, Dataset 1
ProteinaseK, Res 54 (chi1)
Dataset 1
Dataset 6
Normalized Score
χ1
ProteinaseK, Res 54 (chi1)
Pearson r: 0.767
Normalized Score, Dataset 6
Normalized Score, Dataset 1
ProteinaseK, Res 63 (chi1)
Dataset 1
Dataset 6
Normalized Score
χ1
ProteinaseK, Res 63 (chi1)
Pearson r: 0.906
Normalized Score, Dataset 6
Normalized Score, Dataset 1
ProteinaseK, Res 67 (chi1)
Dataset 1
Dataset 6
Normalized Score
χ1
ProteinaseK, Res 67 (chi1)
Pearson r: 0 9457
Normalized Score, Dataset 6
Normalized Score, Dataset 1
ProteinaseK, Res 69 (chi1)
Dataset 1
Dataset 6
Normalized Score
χ1
ProteinaseK, Res 69 (chi1)
Pearson r: 0 9395
Normalized Score, Dataset 6
Normalized Score, Dataset 1
ProteinaseK, Res 101 (chi1)
Dataset 1
Dataset 6
Normalized Score
χ1
ProteinaseK, Res 101 (chi1)
Pearson r: 0.621
Normalized Score, Dataset 6
Normalized Score, Dataset 1
ProteinaseK, Res 112 (chi1)
Dataset 1
Dataset 6
Normalized Score
χ1
ProteinaseK, Res 112 (chi1)
Pearson r: 0.6907
Normalized Score, Dataset 6
Normalized Score, Dataset 1
ProteinaseK, Res 121 (chi1)
Dataset 1
Dataset 6
Normalized Score
χ1
ProteinaseK, Res 121 (chi1)
Pearson r: 0.9179
Normalized Score, Dataset 6
Normalized Score, Dataset 1
ProteinaseK, Res 137 (chi1)
Dataset 1
Dataset 6
Normalized Score
χ1
ProteinaseK, Res 137 (chi1)
Pearson r: 0.9393
Normalized Score, Dataset 6
Normalized Score, Dataset 1
ProteinaseK, Res 139 (chi1)
Dataset 1
Dataset 6
Normalized Score
χ1
ProteinaseK, Res 139 (chi1)
Pearson r: 0.9488
Normalized Score, Dataset 6
Normalized Score, Dataset 1

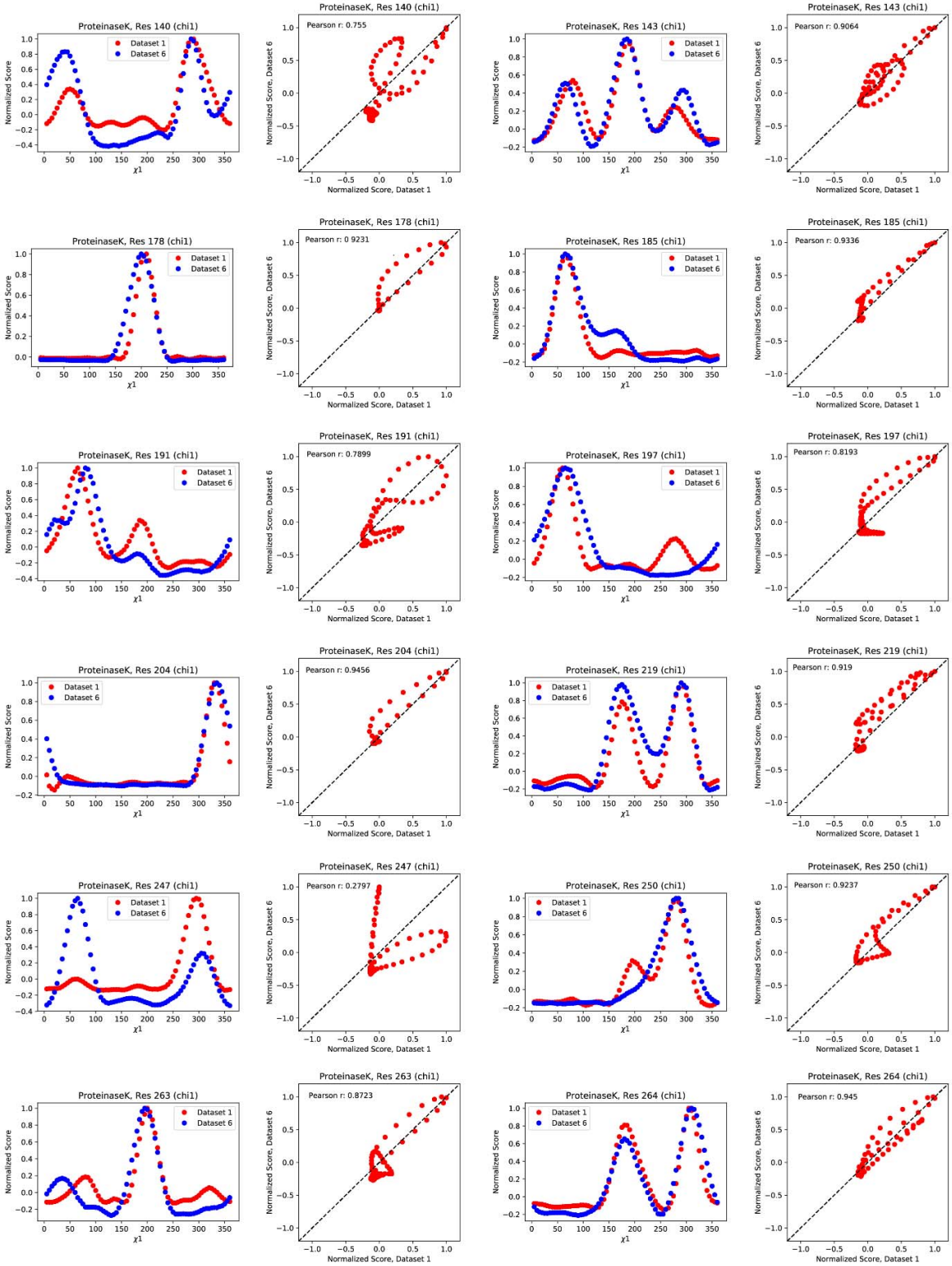
ProteinaseK, Res 140 (chi1)
Dataset 1
Dataset 6
Normalized Score
χ1
ProteinaseK, Res 140 (chi1)
Pearson r: 0.755
Normalized Score, Dataset 6
Normalized Score, Dataset 1
ProteinaseK, Res 143 (chi1)
Dataset 1
Dataset 6
Normalized Score
χ1
ProteinaseK, Res 143 (chi1)
Pearson r: 0.9064
Normalized Score, Dataset 6
Normalized Score, Dataset 1
ProteinaseK, Res 178 (chi1)
Dataset 1
Dataset 6
Normalized Score
χ1
ProteinaseK, Res 178 (chi1)
Pearson r: 0.9231
Normalized Score, Dataset 6
Normalized Score, Dataset 1
ProteinaseK, Res 185 (chi1)
Dataset 1
Dataset 6
Normalized Score
χ1
ProteinaseK, Res 185 (chi1)
Pearson r: 0.9336
Normalized Score, Dataset 6
Normalized Score, Dataset 1
ProteinaseK, Res 191 (chi1)
Dataset 1
Dataset 6
Normalized Score
χ1
ProteinaseK, Res 191 (chi1)
Pearson r: 0.7899
Normalized Score, Dataset 6
Normalized Score, Dataset 1
ProteinaseK, Res 197 (chi1)
Dataset 1
Dataset 6
Normalized Score
χ1
ProteinaseK, Res 197 (chi1)
Pearson r: 0.8193
Normalized Score, Dataset 6
Normalized Score, Dataset 1
ProteinaseK, Res 204 (chi1)
Dataset 1
Dataset 6
Normalized Score
χ1
ProteinaseK, Res 204 (chi1)
Pearson r: 0.9456
Normalized Score, Dataset 6
Normalized Score, Dataset 1
ProteinaseK, Res 219 (chi1)
Dataset 1
Dataset 6
Normalized Score
χ1
ProteinaseK, Res 219 (chi1)
Pearson r: 0.919
Normalized Score, Dataset 6
Normalized Score, Dataset 1
ProteinaseK, Res 247 (chi1)
Dataset 1
Dataset 6
Normalized Score
χ1
ProteinaseK, Res 247 (chi1)
Pearson r: 0.2797
Normalized Score, Dataset 6
Normalized Score, Dataset 1
ProteinaseK, Res 250 (chi1)
Dataset 1
Dataset 6
Normalized Score
χ1
ProteinaseK, Res 250 (chi1)
Pearson r: 0.9237
Normalized Score, Dataset 6
Normalized Score, Dataset 1
ProteinaseK, Res 263 (chi1)
Dataset 1
Dataset 6
Normalized Score
χ1
ProteinaseK, Res 263 (chi1)
Pearson r: 0.8723
Normalized Score, Dataset 6
Normalized Score, Dataset 1
ProteinaseK, Res 264 (chi1)
Dataset 1
Dataset 6
Normalized Score
χ1
ProteinaseK, Res 264 (chi1)
Pearson r: 0.945
Normalized Score, Dataset 6
Normalized Score, Dataset 1

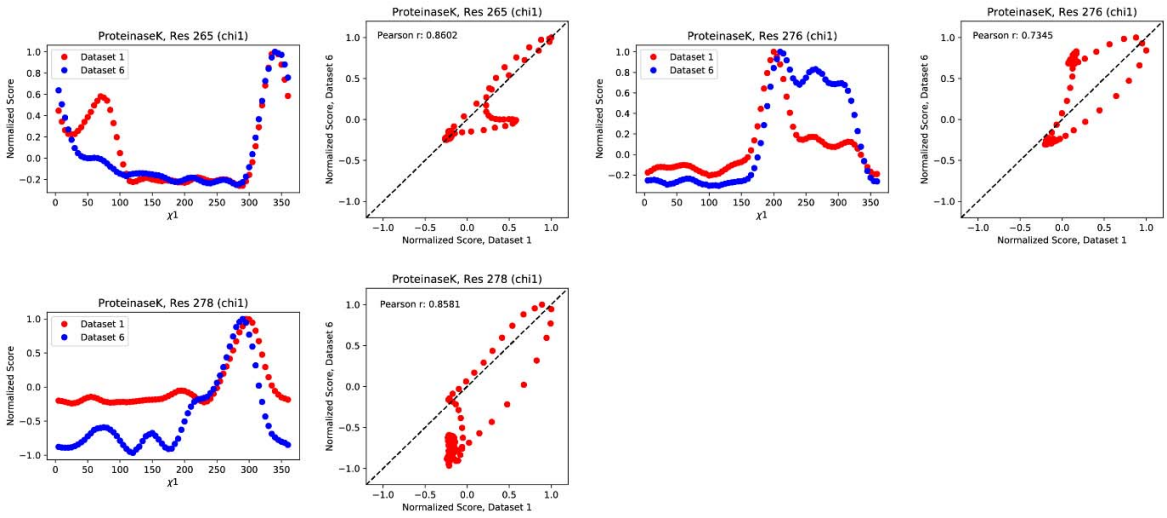

Figure S17 Normalized *Ringer* profiles with Pearson correlation coefficients (PCC) ≤ 0.95 from proteinase K 100 K data for dataset 1 (red) and dataset 6 (blue). Also shown are the associated correlation plots and respective PCC values.

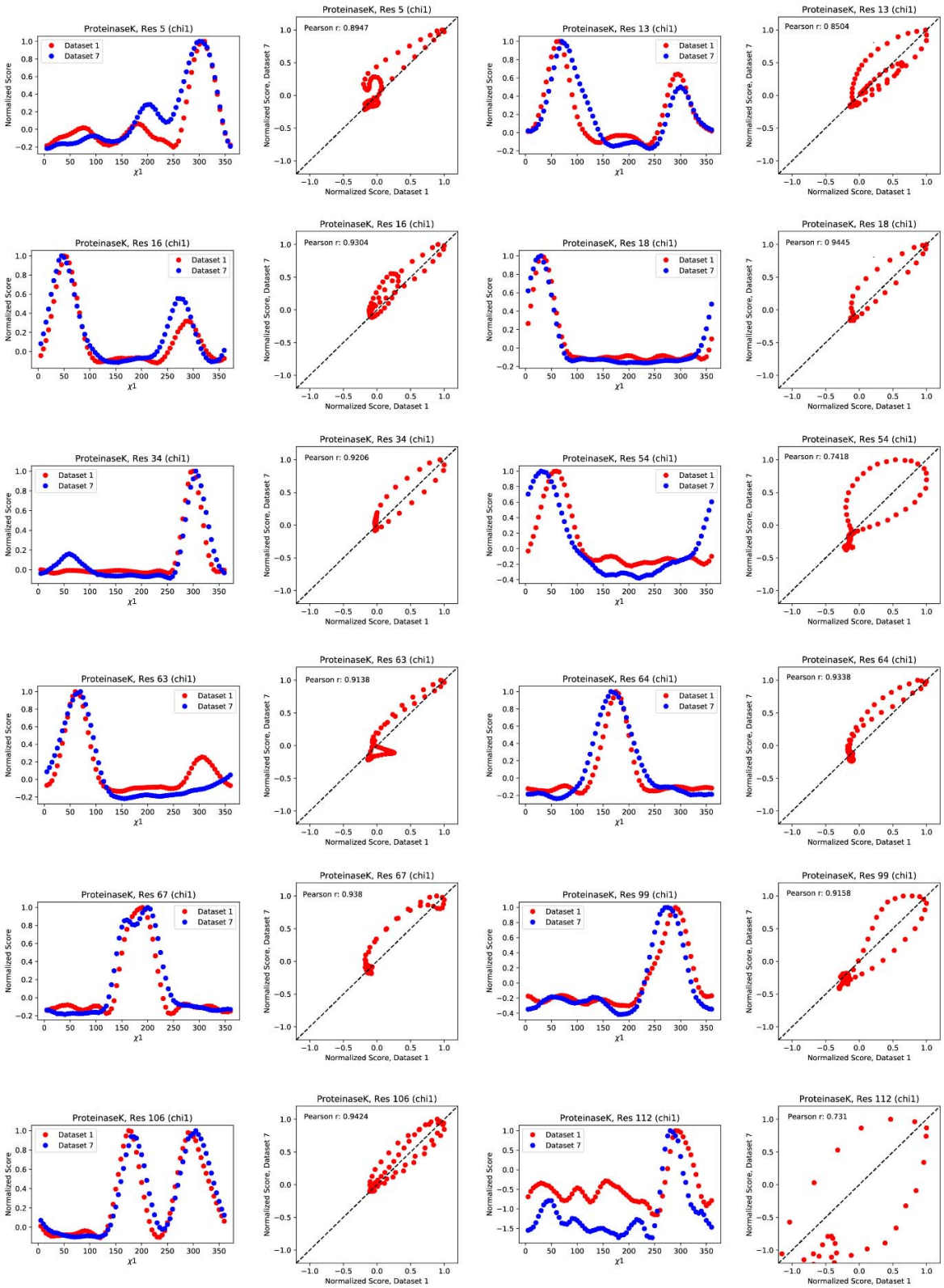
ProteinaseK, Res 5 (chi1)
Dataset 1
Dataset 7
Normalized Score
χ1
ProteinaseK, Res 5 (chi1)
Pearson r: 0.8947
Normalized Score, Dataset 7
Normalized Score, Dataset 1
ProteinaseK, Res 13 (chi1)
Dataset 1
Dataset 7
Normalized Score
χ1
ProteinaseK, Res 13 (chi1)
Pearson r: 0 8504
Normalized Score, Dataset 7
Normalized Score, Dataset 1
ProteinaseK, Res 16 (chi1)
Dataset 1
Dataset 7
Normalized Score
χ1
ProteinaseK, Res 16 (chi1)
Pearson r: 0.9304
Normalized Score, Dataset 7
Normalized Score, Dataset 1
ProteinaseK, Res 18 (chi1)
Dataset 1
Dataset 7
Normalized Score
χ1
ProteinaseK, Res 18 (chi1)
Pearson r: 0 9445
Normalized Score, Dataset 7
Normalized Score, Dataset 1
ProteinaseK, Res 34 (chi1)
Dataset 1
Dataset 7
Normalized Score
χ1
ProteinaseK, Res 34 (chi1)
Pearson r: 0.9206
Normalized Score, Dataset 7
Normalized Score, Dataset 1
ProteinaseK, Res 54 (chi1)
Dataset 1
Dataset 7
Normalized Score
χ1
ProteinaseK, Res 54 (chi1)
Pearson r: 0.7418
Normalized Score, Dataset 7
Normalized Score, Dataset 1
ProteinaseK, Res 63 (chi1)
Dataset 1
Dataset 7
Normalized Score
χ1
ProteinaseK, Res 63 (chi1)
Pearson r: 0.9138
Normalized Score, Dataset 7
Normalized Score, Dataset 1
ProteinaseK, Res 64 (chi1)
Dataset 1
Dataset 7
Normalized Score
χ1
ProteinaseK, Res 64 (chi1)
Pearson r: 0.9338
Normalized Score, Dataset 7
Normalized Score, Dataset 1
ProteinaseK, Res 67 (chi1)
Dataset 1
Dataset 7
Normalized Score
χ1
ProteinaseK, Res 67 (chi1)
Pearson r: 0.938
Normalized Score, Dataset 7
Normalized Score, Dataset 1
ProteinaseK, Res 99 (chi1)
Dataset 1
Dataset 7
Normalized Score
χ1
ProteinaseK, Res 99 (chi1)
Pearson r: 0.9158
Normalized Score, Dataset 7
Normalized Score, Dataset 1
ProteinaseK, Res 106 (chi1)
Dataset 1
Dataset 7
Normalized Score
χ1
ProteinaseK, Res 106 (chi1)
Pearson r: 0.9424
Normalized Score, Dataset 7
Normalized Score, Dataset 1
ProteinaseK, Res 112 (chi1)
Dataset 1
Dataset 7
Normalized Score
χ1
ProteinaseK, Res 112 (chi1)
Pearson r: 0.731
Normalized Score, Dataset 7
Normalized Score, Dataset 1

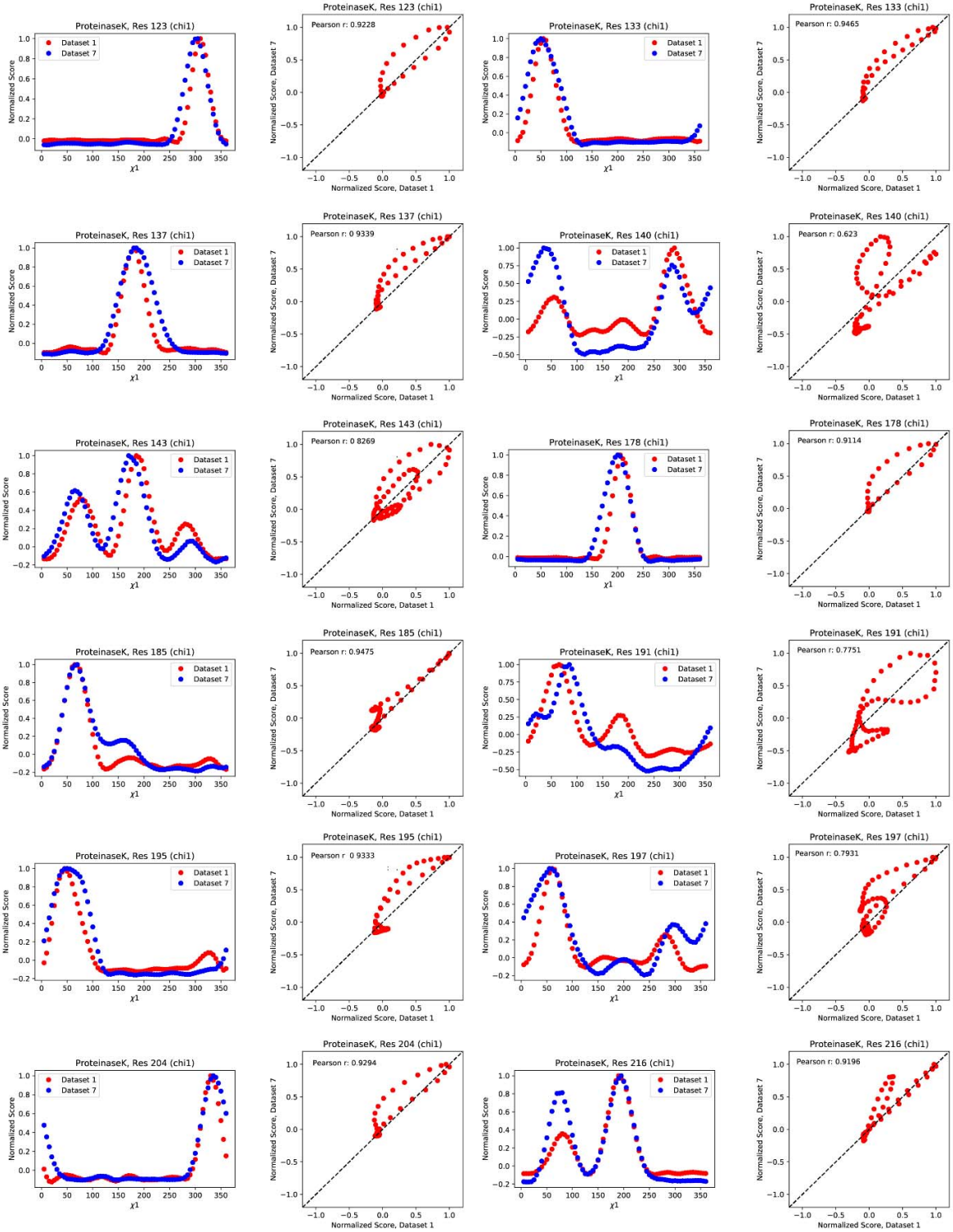
ProteinaseK, Res 123 (chi1)
Dataset 1
Dataset 7
Normalized Score
χ1
ProteinaseK, Res 123 (chi1)
Pearson r: 0.9228
Normalized Score, Dataset 7
Normalized Score, Dataset 1
ProteinaseK, Res 133 (chi1)
Dataset 1
Dataset 7
Normalized Score
χ1
ProteinaseK, Res 133 (chi1)
Pearson r: 0.9465
Normalized Score, Dataset 7
Normalized Score, Dataset 1
ProteinaseK, Res 137 (chi1)
Dataset 1
Dataset 7
Normalized Score
χ1
ProteinaseK, Res 137 (chi1)
Pearson r: 0 9339
Normalized Score, Dataset 7
Normalized Score, Dataset 1
ProteinaseK, Res 140 (chi1)
Dataset 1
Dataset 7
Normalized Score
χ1
ProteinaseK, Res 140 (chi1)
Pearson r: 0.623
Normalized Score, Dataset 7
Normalized Score, Dataset 1
ProteinaseK, Res 143 (chi1)
Dataset 1
Dataset 7
Normalized Score
χ1
ProteinaseK, Res 143 (chi1)
Pearson r: 0 8269
Normalized Score, Dataset 7
Normalized Score, Dataset 1
ProteinaseK, Res 178 (chi1)
Dataset 1
Dataset 7
Normalized Score
χ1
ProteinaseK, Res 178 (chi1)
Pearson r: 0.9114
Normalized Score, Dataset 7
Normalized Score, Dataset 1
ProteinaseK, Res 185 (chi1)
Dataset 1
Dataset 7
Normalized Score
χ1
ProteinaseK, Res 185 (chi1)
Pearson r: 0.9475
Normalized Score, Dataset 7
Normalized Score, Dataset 1
ProteinaseK, Res 191 (chi1)
Dataset 1
Dataset 7
Normalized Score
χ1
ProteinaseK, Res 191 (chi1)
Pearson r: 0.7751
Normalized Score, Dataset 7
Normalized Score, Dataset 1
ProteinaseK, Res 195 (chi1)
Dataset 1
Dataset 7
Normalized Score
χ1
ProteinaseK, Res 195 (chi1)
Pearson r 0 9333
Normalized Score, Dataset 7
Normalized Score, Dataset 1
ProteinaseK, Res 197 (chi1)
Dataset 1
Dataset 7
Normalized Score
χ1
ProteinaseK, Res 197 (chi1)
Pearson r: 0.7931
Normalized Score, Dataset 7
Normalized Score, Dataset 1
ProteinaseK, Res 204 (chi1)
Dataset 1
Dataset 7
Normalized Score
χ1
ProteinaseK, Res 204 (chi1)
Pearson r: 0.9294
Normalized Score, Dataset 7
Normalized Score, Dataset 1
ProteinaseK, Res 216 (chi1)
Dataset 1
Dataset 7
Normalized Score
χ1
ProteinaseK, Res 216 (chi1)
Pearson r: 0.9196
Normalized Score, Dataset 7
Normalized Score, Dataset 1

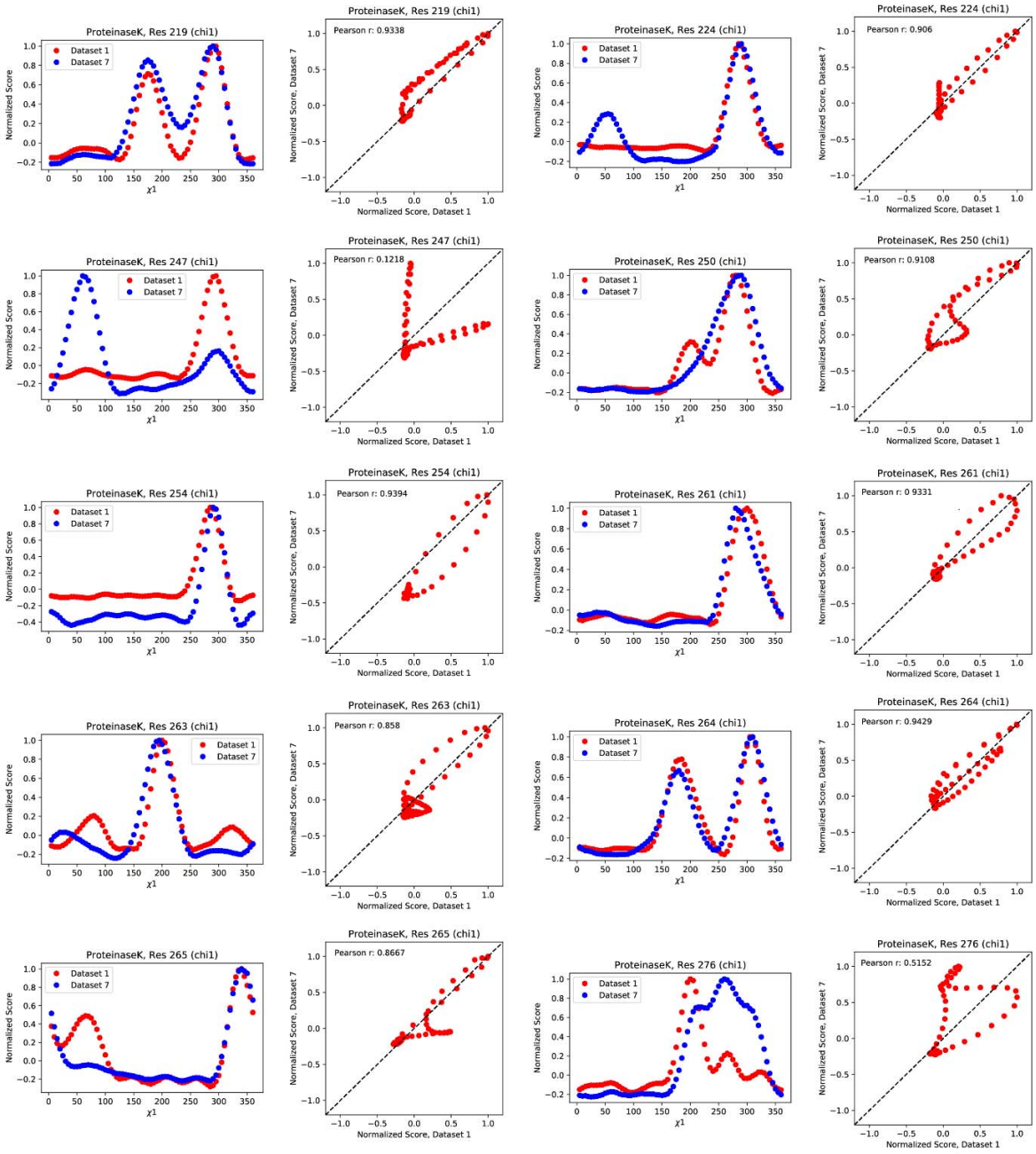

Figure S18 Normalized *Ringer* profiles with Pearson correlation coefficients (PCC) $\leq$ 0.95 from proteinase K 100 K data for dataset 1 (red) and dataset 7 (blue). Also shown are the associated correlation plots and respective PCC values.

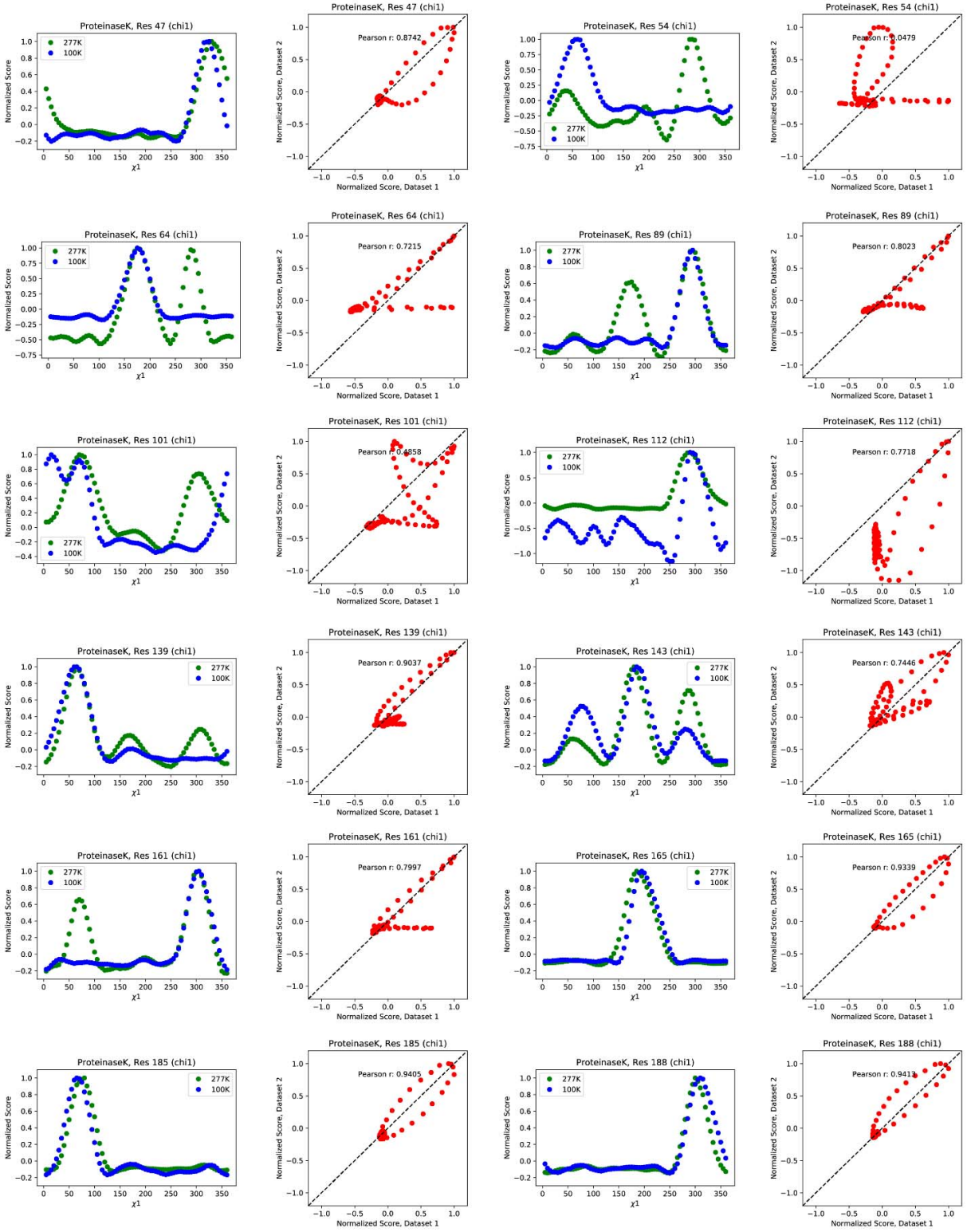
ProteinaseK, Res 47 (chi1)
277K
100K
Normalized Score
χ1
ProteinaseK, Res 47 (chi1)
Pearson r: 0.8742
Normalized Score, Dataset 2
Normalized Score, Dataset 1
ProteinaseK, Res 54 (chi1)
277K
100K
Normalized Score
χ1
ProteinaseK, Res 54 (chi1)
Pearson r: 0.0479
Normalized Score, Dataset 2
Normalized Score, Dataset 1
ProteinaseK, Res 64 (chi1)
277K
100K
Normalized Score
χ1
ProteinaseK, Res 64 (chi1)
Pearson r: 0.7215
Normalized Score, Dataset 2
Normalized Score, Dataset 1
ProteinaseK, Res 89 (chi1)
277K
100K
Normalized Score
χ1
ProteinaseK, Res 89 (chi1)
Pearson r: 0.8023
Normalized Score, Dataset 2
Normalized Score, Dataset 1
ProteinaseK, Res 101 (chi1)
277K
100K
Normalized Score
χ1
ProteinaseK, Res 101 (chi1)
Pearson r: 0.4858
Normalized Score, Dataset 2
Normalized Score, Dataset 1
ProteinaseK, Res 112 (chi1)
277K
100K
Normalized Score
χ1
ProteinaseK, Res 112 (chi1)
Pearson r: 0.7718
Normalized Score, Dataset 2
Normalized Score, Dataset 1
ProteinaseK, Res 139 (chi1)
277K
100K
Normalized Score
χ1
ProteinaseK, Res 139 (chi1)
Pearson r: 0.9037
Normalized Score, Dataset 2
Normalized Score, Dataset 1
ProteinaseK, Res 143 (chi1)
277K
100K
Normalized Score
χ1
ProteinaseK, Res 143 (chi1)
Pearson r: 0.7446
Normalized Score, Dataset 2
Normalized Score, Dataset 1
ProteinaseK, Res 161 (chi1)
277K
100K
Normalized Score
χ1
ProteinaseK, Res 161 (chi1)
Pearson r: 0.7997
Normalized Score, Dataset 2
Normalized Score, Dataset 1
ProteinaseK, Res 165 (chi1)
277K
100K
Normalized Score
χ1
ProteinaseK, Res 165 (chi1)
Pearson r: 0.9339
Normalized Score, Dataset 2
Normalized Score, Dataset 1
ProteinaseK, Res 185 (chi1)
277K
100K
Normalized Score
χ1
ProteinaseK, Res 185 (chi1)
Pearson r: 0.9405
Normalized Score, Dataset 2
Normalized Score, Dataset 1
ProteinaseK, Res 188 (chi1)
277K
100K
Normalized Score
χ1
ProteinaseK, Res 188 (chi1)
Pearson r: 0.9413
Normalized Score, Dataset 2
Normalized Score, Dataset 1

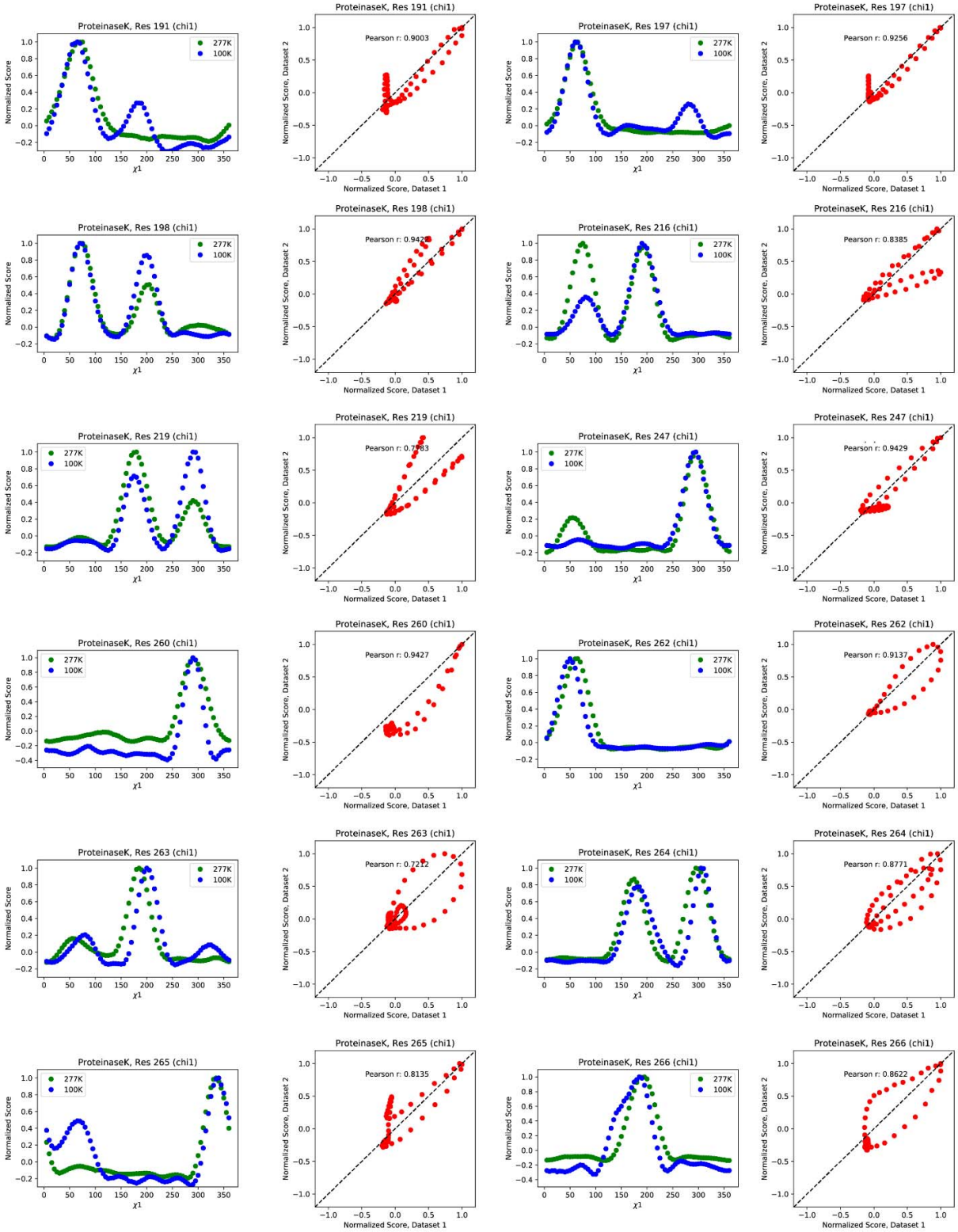
ProteinaseK, Res 191 (chi1)
277K
100K
Normalized Score
χ1
ProteinaseK, Res 191 (chi1)
Pearson r: 0.9003
Normalized Score, Dataset 1
Normalized Score, Dataset 2
ProteinaseK, Res 197 (chi1)
277K
100K
Normalized Score
χ1
ProteinaseK, Res 197 (chi1)
Pearson r: 0.9256
Normalized Score, Dataset 1
Normalized Score, Dataset 2
ProteinaseK, Res 198 (chi1)
277K
100K
Normalized Score
χ1
ProteinaseK, Res 198 (chi1)
Pearson r: 0.942
Normalized Score, Dataset 1
Normalized Score, Dataset 2
ProteinaseK, Res 216 (chi1)
277K
100K
Normalized Score
χ1
ProteinaseK, Res 216 (chi1)
Pearson r: 0.8385
Normalized Score, Dataset 1
Normalized Score, Dataset 2
ProteinaseK, Res 219 (chi1)
277K
100K
Normalized Score
χ1
ProteinaseK, Res 219 (chi1)
Pearson r: 0.7583
Normalized Score, Dataset 1
Normalized Score, Dataset 2
ProteinaseK, Res 247 (chi1)
277K
100K
Normalized Score
χ1
ProteinaseK, Res 247 (chi1)
Pearson r: 0.9429
Normalized Score, Dataset 1
Normalized Score, Dataset 2
ProteinaseK, Res 260 (chi1)
277K
100K
Normalized Score
χ1
ProteinaseK, Res 260 (chi1)
Pearson r: 0.9427
Normalized Score, Dataset 1
Normalized Score, Dataset 2
ProteinaseK, Res 262 (chi1)
277K
100K
Normalized Score
χ1
ProteinaseK, Res 262 (chi1)
Pearson r: 0.9137
Normalized Score, Dataset 1
Normalized Score, Dataset 2
ProteinaseK, Res 263 (chi1)
277K
100K
Normalized Score
χ1
ProteinaseK, Res 263 (chi1)
Pearson r: 0.7212
Normalized Score, Dataset 1
Normalized Score, Dataset 2
ProteinaseK, Res 264 (chi1)
277K
100K
Normalized Score
χ1
ProteinaseK, Res 264 (chi1)
Pearson r: 0.8771
Normalized Score, Dataset 1
Normalized Score, Dataset 2
ProteinaseK, Res 265 (chi1)
277K
100K
Normalized Score
χ1
ProteinaseK, Res 265 (chi1)
Pearson r: 0.8135
Normalized Score, Dataset 1
Normalized Score, Dataset 2
ProteinaseK, Res 266 (chi1)
277K
100K
Normalized Score
χ1
ProteinaseK, Res 266 (chi1)
Pearson r: 0.8622
Normalized Score, Dataset 1
Normalized Score, Dataset 2

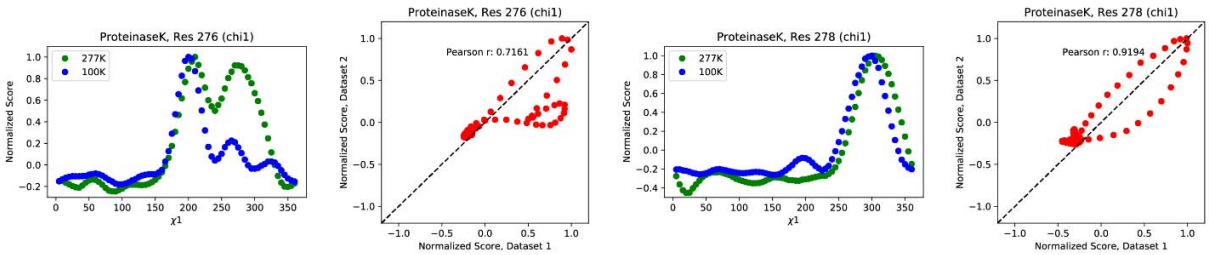

Figure S19 Normalized *Ringer* profiles for the proteinase K 277 K least damaged dataset 1 (green) and the 100 K least damaged dataset 1 (blue) with Pearson correlation coefficients (PCC) ≤ 0.95. Also shown are the associated correlation plots and respective PCC values.

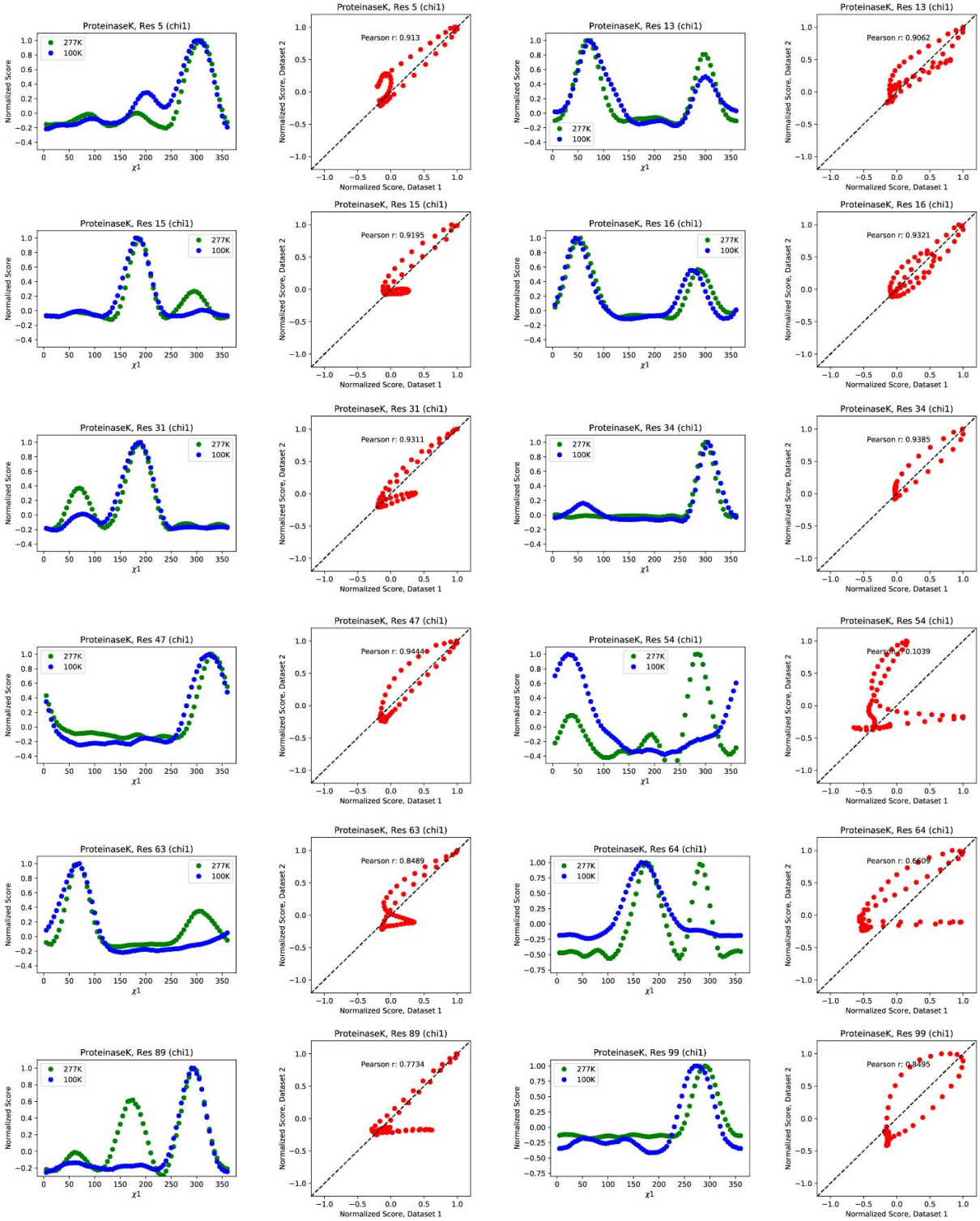
ProteinaseK, Res 5 (chi1)
277K
100K
Normalized Score
χ1
ProteinaseK, Res 5 (chi1)
Pearson r: 0.913
Normalized Score, Dataset 2
Normalized Score, Dataset 1
ProteinaseK, Res 13 (chi1)
277K
100K
Normalized Score
χ1
ProteinaseK, Res 13 (chi1)
Pearson r: 0.9062
Normalized Score, Dataset 2
Normalized Score, Dataset 1
ProteinaseK, Res 15 (chi1)
277K
100K
Normalized Score
χ1
ProteinaseK, Res 15 (chi1)
Pearson r: 0.9195
Normalized Score, Dataset 2
Normalized Score, Dataset 1
ProteinaseK, Res 16 (chi1)
277K
100K
Normalized Score
χ1
ProteinaseK, Res 16 (chi1)
Pearson r: 0.9321
Normalized Score, Dataset 2
Normalized Score, Dataset 1
ProteinaseK, Res 31 (chi1)
277K
100K
Normalized Score
χ1
ProteinaseK, Res 31 (chi1)
Pearson r: 0.9311
Normalized Score, Dataset 2
Normalized Score, Dataset 1
ProteinaseK, Res 34 (chi1)
277K
100K
Normalized Score
χ1
ProteinaseK, Res 34 (chi1)
Pearson r: 0.9385
Normalized Score, Dataset 2
Normalized Score, Dataset 1
ProteinaseK, Res 47 (chi1)
277K
100K
Normalized Score
χ1
ProteinaseK, Res 47 (chi1)
Pearson r: 0.9444
Normalized Score, Dataset 2
Normalized Score, Dataset 1
ProteinaseK, Res 54 (chi1)
277K
100K
Normalized Score
χ1
ProteinaseK, Res 54 (chi1)
Pearson r: 0.1039
Normalized Score, Dataset 2
Normalized Score, Dataset 1
ProteinaseK, Res 63 (chi1)
277K
100K
Normalized Score
χ1
ProteinaseK, Res 63 (chi1)
Pearson r: 0.8489
Normalized Score, Dataset 2
Normalized Score, Dataset 1
ProteinaseK, Res 64 (chi1)
277K
100K
Normalized Score
χ1
ProteinaseK, Res 64 (chi1)
Pearson r: 0.6609
Normalized Score, Dataset 2
Normalized Score, Dataset 1
ProteinaseK, Res 89 (chi1)
277K
100K
Normalized Score
χ1
ProteinaseK, Res 89 (chi1)
Pearson r: 0.7734
Normalized Score, Dataset 2
Normalized Score, Dataset 1
ProteinaseK, Res 99 (chi1)
277K
100K
Normalized Score
χ1
ProteinaseK, Res 99 (chi1)
Pearson r: 0.8495
Normalized Score, Dataset 2
Normalized Score, Dataset 1

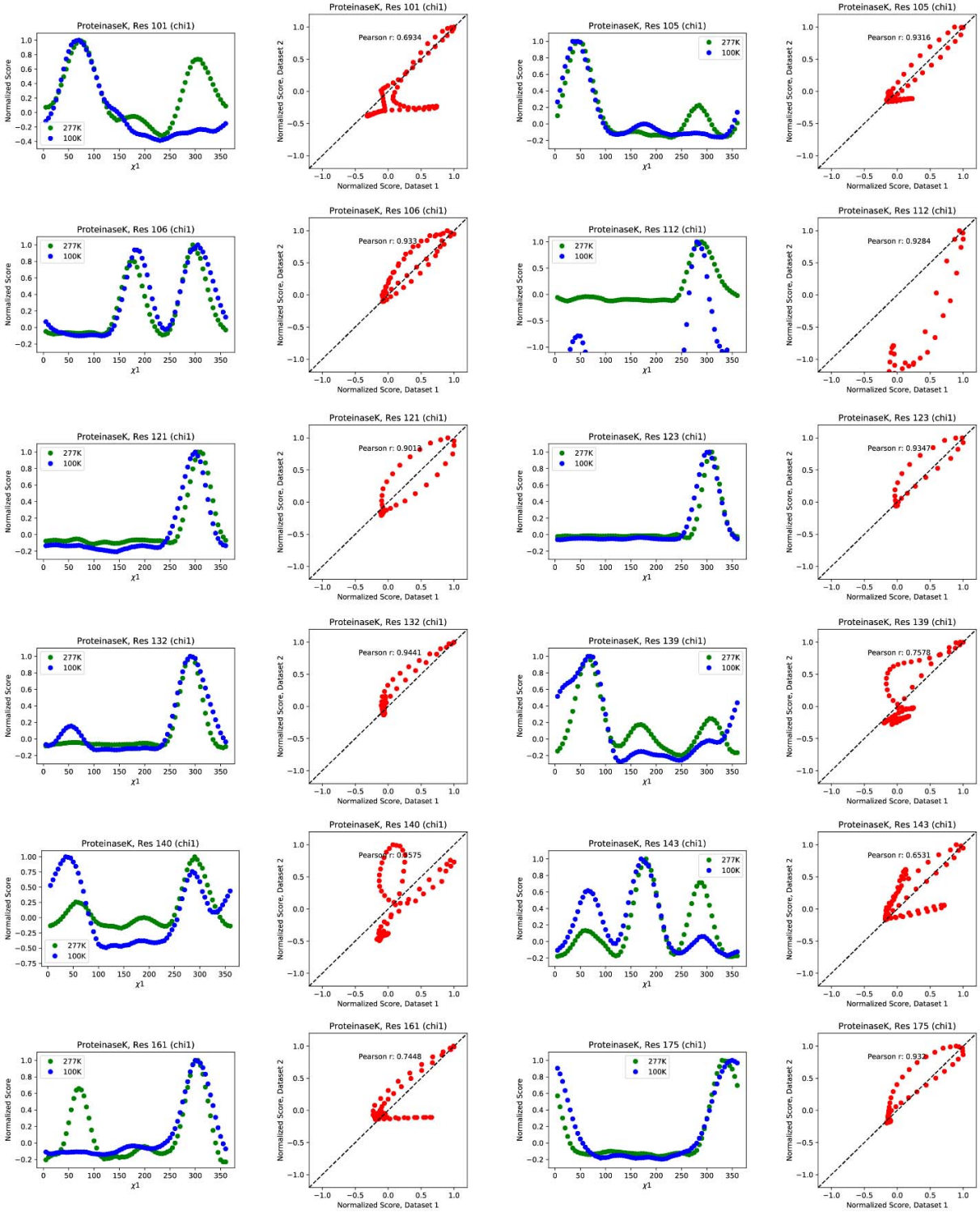
ProteinaseK, Res 101 (chi1)
Pearson r: 0.6934
ProteinaseK, Res 105 (chi1)
Pearson r: 0.9316
ProteinaseK, Res 106 (chi1)
Pearson r: 0.933
ProteinaseK, Res 112 (chi1)
Pearson r: 0.9284
ProteinaseK, Res 121 (chi1)
Pearson r: 0.9013
ProteinaseK, Res 123 (chi1)
Pearson r: 0.9347
ProteinaseK, Res 132 (chi1)
Pearson r: 0.9441
ProteinaseK, Res 139 (chi1)
Pearson r: 0.7578
ProteinaseK, Res 140 (chi1)
Pearson r: 0.9575
ProteinaseK, Res 143 (chi1)
Pearson r: 0.6531
ProteinaseK, Res 161 (chi1)
Pearson r: 0.7448
ProteinaseK, Res 175 (chi1)
Pearson r: 0.932
277K
100K
Normalized Score
χ1
Normalized Score, Dataset 1
Normalized Score, Dataset 2

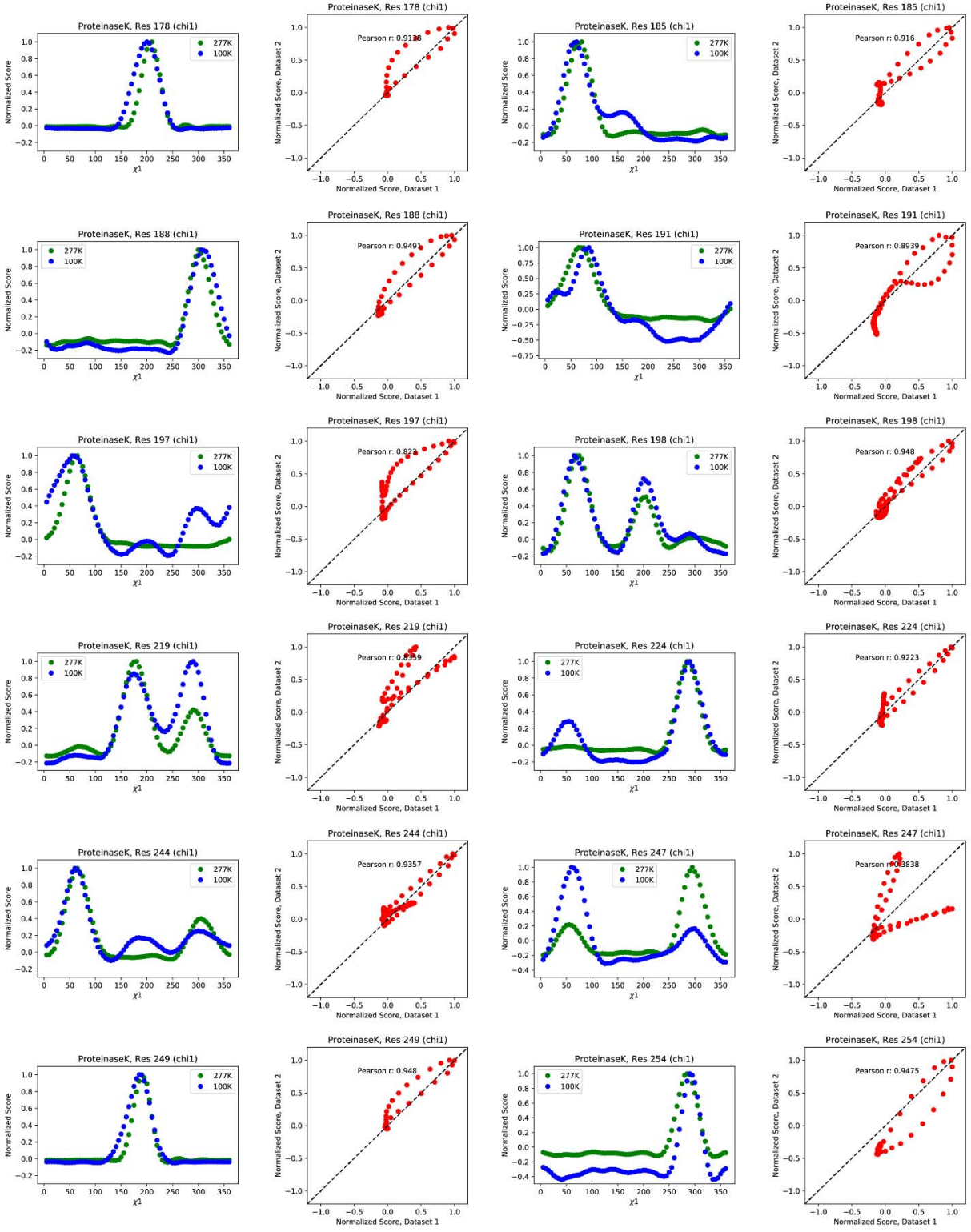
ProteinaseK, Res 178 (chi1)
277K
100K
Normalized Score
χ1
ProteinaseK, Res 178 (chi1)
Pearson r: 0.9138
Normalized Score, Dataset 2
Normalized Score, Dataset 1
ProteinaseK, Res 185 (chi1)
277K
100K
Normalized Score
χ1
ProteinaseK, Res 185 (chi1)
Pearson r: 0.916
Normalized Score, Dataset 2
Normalized Score, Dataset 1
ProteinaseK, Res 188 (chi1)
277K
100K
Normalized Score
χ1
ProteinaseK, Res 188 (chi1)
Pearson r: 0.9491
Normalized Score, Dataset 2
Normalized Score, Dataset 1
ProteinaseK, Res 191 (chi1)
277K
100K
Normalized Score
χ1
ProteinaseK, Res 191 (chi1)
Pearson r: 0.8939
Normalized Score, Dataset 2
Normalized Score, Dataset 1
ProteinaseK, Res 197 (chi1)
277K
100K
Normalized Score
χ1
ProteinaseK, Res 197 (chi1)
Pearson r: 0.823
Normalized Score, Dataset 2
Normalized Score, Dataset 1
ProteinaseK, Res 198 (chi1)
277K
100K
Normalized Score
χ1
ProteinaseK, Res 198 (chi1)
Pearson r: 0.948
Normalized Score, Dataset 2
Normalized Score, Dataset 1
ProteinaseK, Res 219 (chi1)
277K
100K
Normalized Score
χ1
ProteinaseK, Res 219 (chi1)
Pearson r: 0.9359
Normalized Score, Dataset 2
Normalized Score, Dataset 1
ProteinaseK, Res 224 (chi1)
277K
100K
Normalized Score
χ1
ProteinaseK, Res 224 (chi1)
Pearson r: 0.9223
Normalized Score, Dataset 2
Normalized Score, Dataset 1
ProteinaseK, Res 244 (chi1)
277K
100K
Normalized Score
χ1
ProteinaseK, Res 244 (chi1)
Pearson r: 0.9357
Normalized Score, Dataset 2
Normalized Score, Dataset 1
ProteinaseK, Res 247 (chi1)
277K
100K
Normalized Score
χ1
ProteinaseK, Res 247 (chi1)
Pearson r: 0.3838
Normalized Score, Dataset 2
Normalized Score, Dataset 1
ProteinaseK, Res 249 (chi1)
277K
100K
Normalized Score
χ1
ProteinaseK, Res 249 (chi1)
Pearson r: 0.948
Normalized Score, Dataset 2
Normalized Score, Dataset 1
ProteinaseK, Res 254 (chi1)
277K
100K
Normalized Score
χ1
ProteinaseK, Res 254 (chi1)
Pearson r: 0.9475
Normalized Score, Dataset 2
Normalized Score, Dataset 1

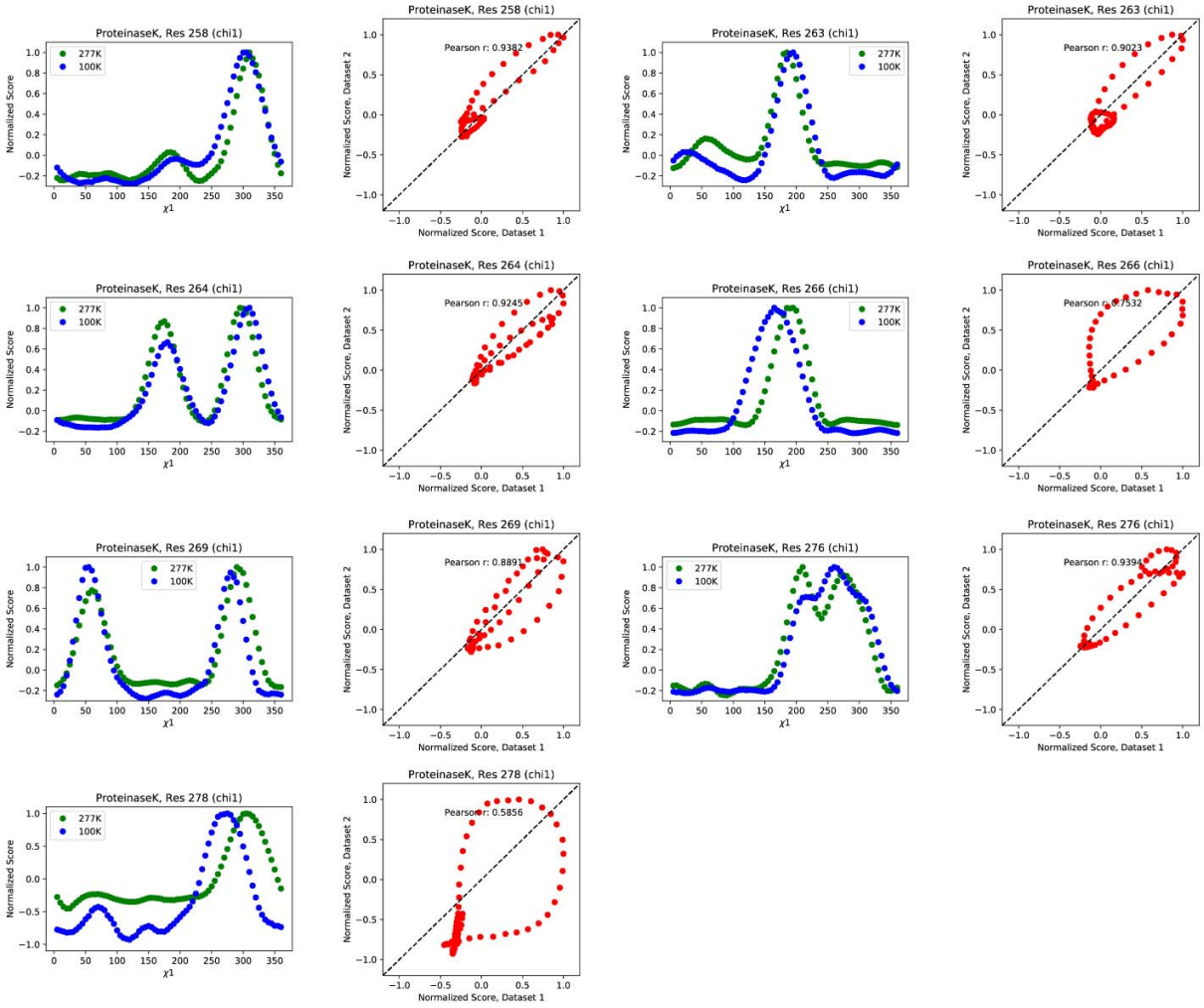

Figure S20 Normalized *Ringer* profiles for the proteinase K 277 K least damaged dataset 1 (green) and the 100 K most damaged dataset 7 (blue) with Pearson correlation coefficients (PCC) ≤ 0.95. Also shown are the associated correlation plots and respective PCC values.

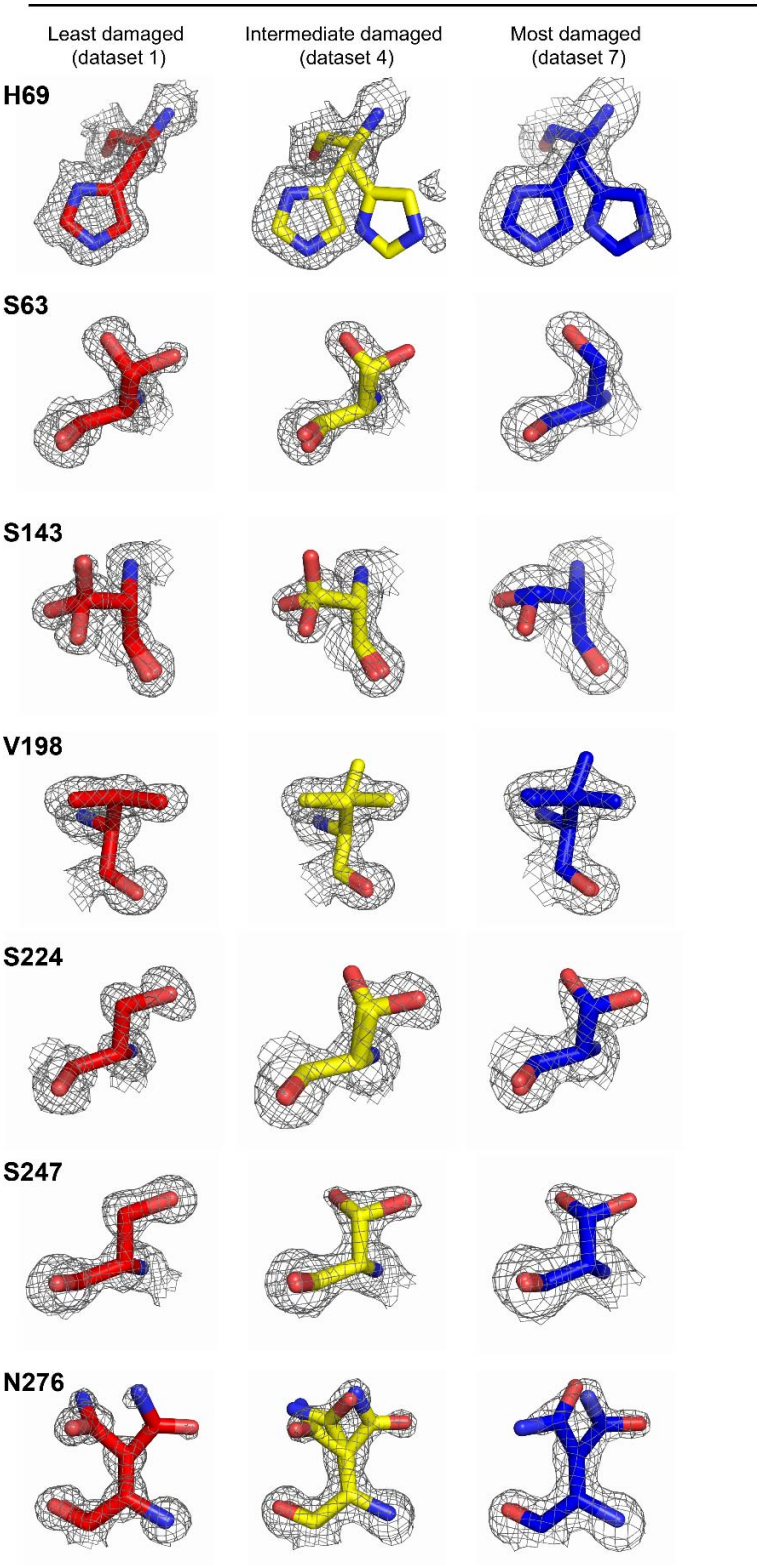
Least damaged
(dataset 1)
Intermediate damaged
(dataset 4)
Most damaged
(dataset 7)
H69
S63
S143
V198
S224
S247
N276

Figure S21 X-ray damage to cryo cooled crystals can alter protein side chain rotameric distributions. The least (dataset 1), intermediate (dataset 4), and most (dataset 7) damaged cryo datasets, residues are shown as sticks. Electron density is shown as grey mesh and is contoured at 1σ for all residues except H69, for which the contour is at 0.4 sigma.

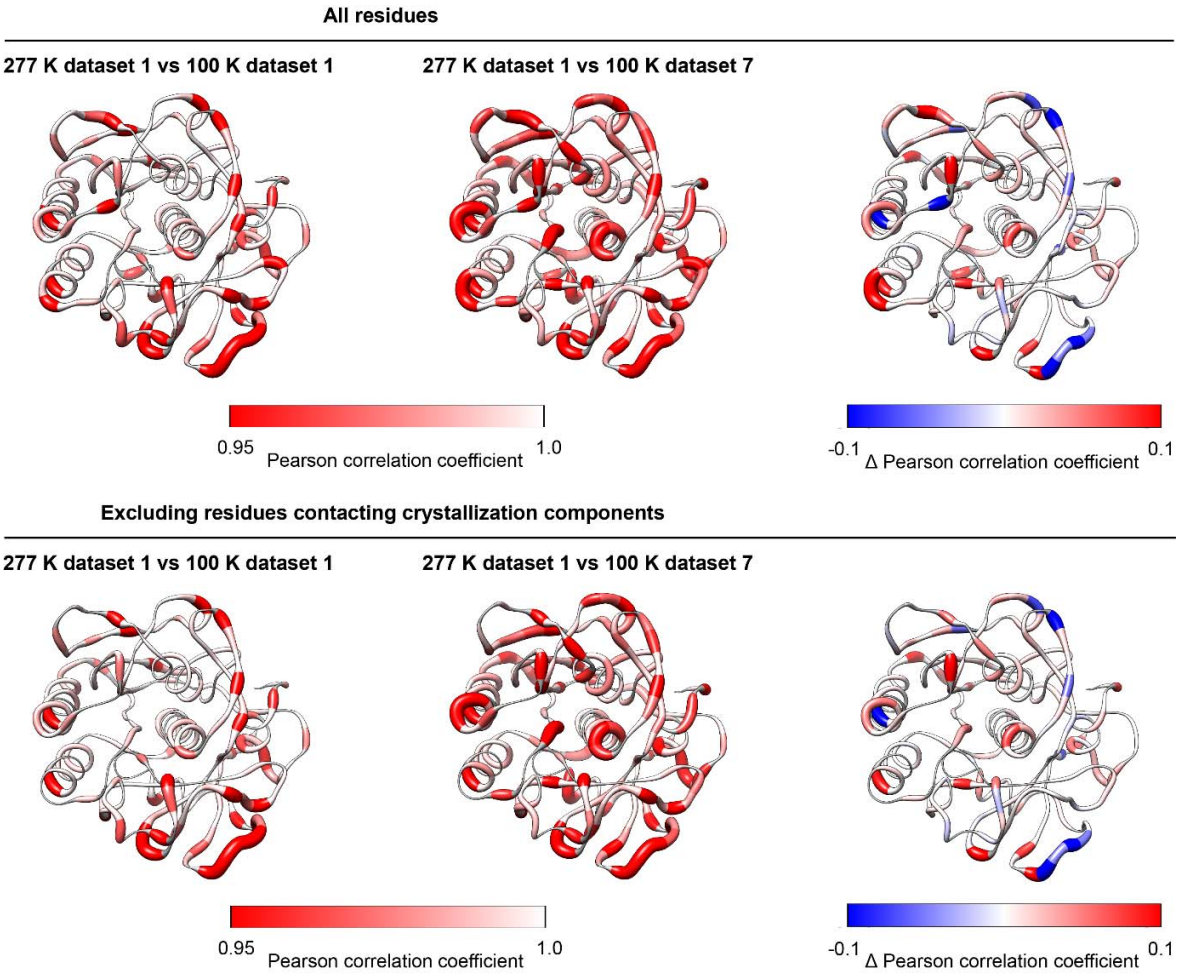

Figure S22 Comparison of P_{CC} values (plotted on the proteinase K structure) between the *Ringer* profiles for residues in the 277 K least X-ray damaged dataset 1 and 100 K least X-ray damaged dataset 1 (left), the 277 K least X-ray damaged dataset 1 and 100 K most X-ray damaged dataset 7 (middle), and the difference (Δ)P_{CC} obtained by subtracting top middle from top left P_{CC} values, plotted on the proteinase K structure (right). All residues with χ1 angles (top) and excluding residues in contact with crystallization components (bottom, see **Table S12**). Residues with no χ1 angles and excluded residues are colored in grey. The diameter of the worm representation is correlated with the magnitude of the P_{CC}.

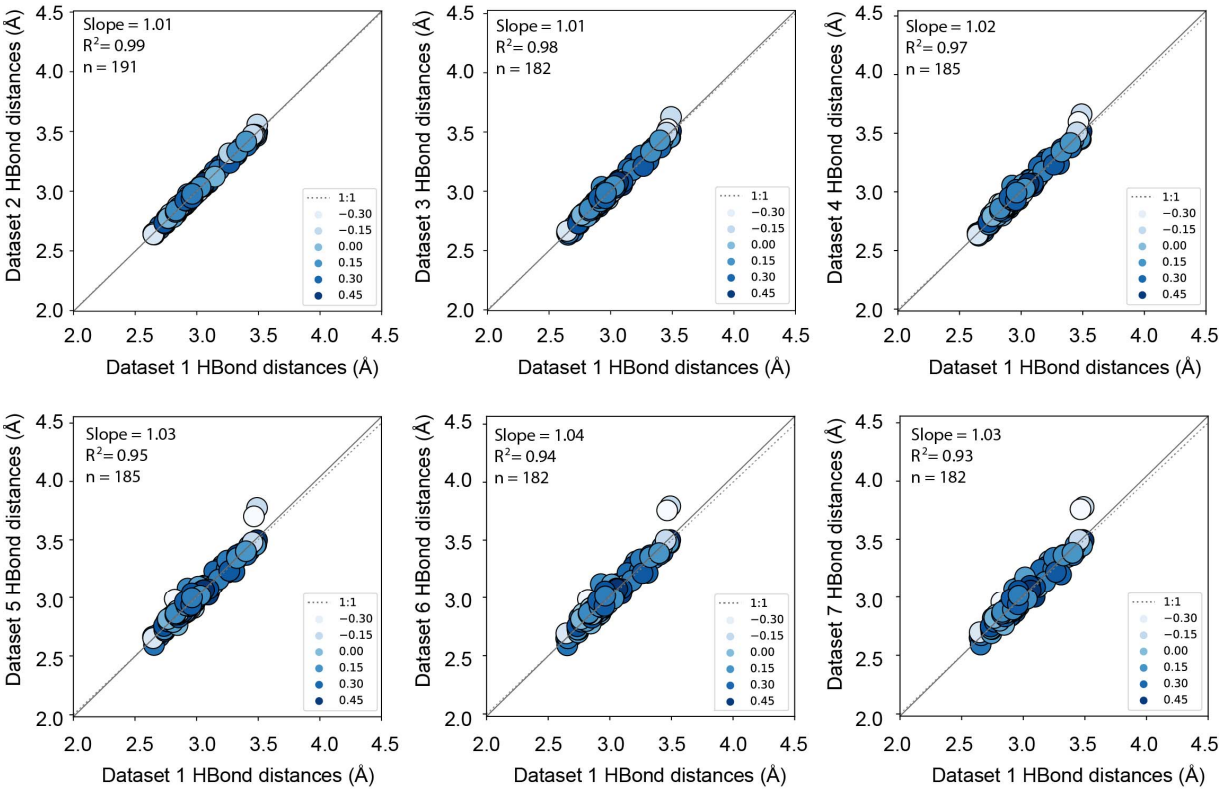

Figure S23 Gradual deterioration of the correlation between measured hydrogen bond lengths in proteinase K with increasing X-ray damage at 100 K. Correlation plots of hydrogen bond lengths obtained from the least (dataset 1) and increasingly X-ray damaged (dataset 2-7) proteinase K datasets at 100 K. Correlation points are colored according to the relative B-factor of the hydrogen bonding groups such that higher values (darker blue) and lower values (white) correspond to atoms with low- and high B-factors relative to the average, respectively (see Materials and Methods). Differences between proteinase K structures are unlikely to be caused by differences in refinement strategy as all structures have been refined using the same refinement parameters and increasingly damaged models have been refined in a highly consistent manner (see Materials and Methods). The analysis excluded all residues with more than one conformation present in the model (see Materials and Methods). Similar results were obtained with all residues included (Figure S24). See *Supplementary file 2* for hydrogen bond length numerical values.

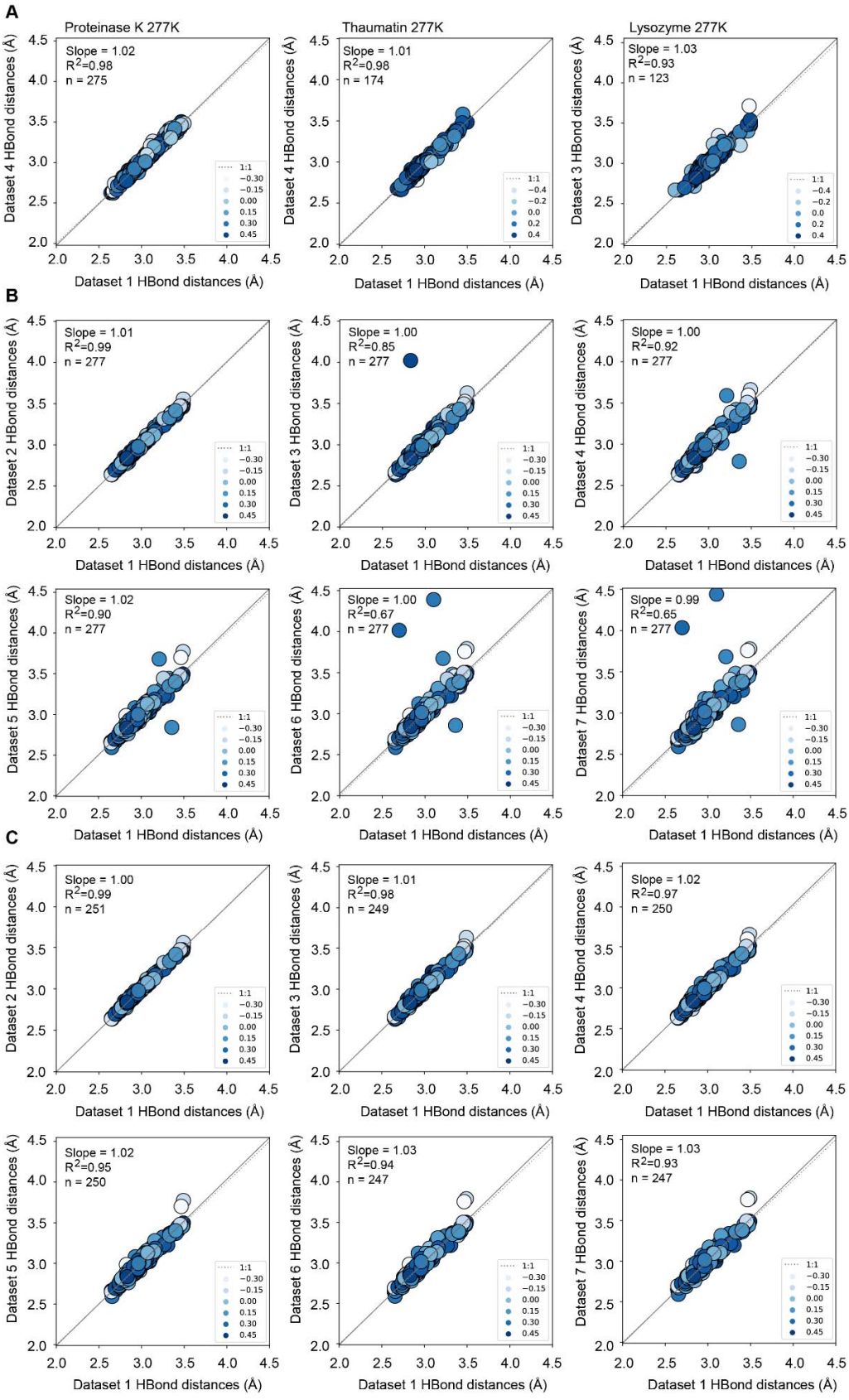
A
Proteinase K 277K
Slope = 1.02
R2=0.98
n = 275
Thaumatin 277K
Slope = 1.01
R2=0.98
n = 174
Lysozyme 277K
Slope = 1.03
R2=0.93
n = 123
B
Slope = 1.01
R2=0.99
n = 277
Slope = 1.00
R2=0.85
n = 277
Slope = 1.00
R2=0.92
n = 277
Slope = 1.02
R2=0.90
n = 277
Slope = 1.00
R2=0.67
n = 277
Slope = 0.99
R2=0.65
n = 277
C
Slope = 1.00
R2=0.99
n = 251
Slope = 1.01
R2=0.98
n = 249
Slope = 1.02
R2=0.97
n = 250
Slope = 1.02
R2=0.95
n = 250
Slope = 1.03
R2=0.94
n = 247
Slope = 1.03
R2=0.93
n = 247
Dataset 1 HBond distances (Å)
Dataset 2 HBond distances (Å)
Dataset 3 HBond distances (Å)
Dataset 4 HBond distances (Å)
Dataset 5 HBond distances (Å)
Dataset 6 HBond distances (Å)
Dataset 7 HBond distances (Å)
1:1

Figure S24 X-ray damage impacts the determination of hydrogen bond lengths in proteinase K more at cryo temperature than at room temperature. (A) Correlation plots of hydrogen bond lengths obtained from the least and most damaged datasets at room temperature. Correlation points are colored according to the relative B-factor of the hydrogen bonding groups such that higher values (darker blue) and lower values (white) correspond to atoms with low- and high B-factors relative to the average, respectively (see Materials and Methods). (B) Correlation plots of hydrogen bond lengths obtained from the least (dataset 1) and increasingly X-ray damaged (dataset 2-7) proteinase K datasets at 100 K. Colors used as in (A). (A) and (B) analyses included all residues and average values are plotted for residues with more than one conformation present in the model (see Materials and Methods). (C) Correlation plots of hydrogen bond lengths obtained from the least (dataset 1) and increasingly X-ray damaged (dataset 2-7) proteinase K datasets at 100 K. The analysis excluded all side chains with more than one conformation present in the model but included average values for backbone hydrogen bonding groups with more than one conformation (see Materials and Methods). Colors used as in (A). See Supplementary file 2 for hydrogen bond length numerical values.

Thaumatin 277 K diffraction data collection statistics				
Batch	1	2	3	4
Wavelength (Å)	0.88557			
Resolution range (Å)	38-26-1.22 (1.24-1.22)	38.28-1.29 (1.31-1.29)	38.29-1.38 (1.40-1.38)	38.29-1.48 (1.51-1.48)
Average diffraction weighted dose (MGy)	0.016	0.114	0.212	0.310
Space group	$P4_12_12$			
Unit cell a (Å), b (Å), c (Å), α (°), β (°), γ (°)	58.81 58.81 151.17 90.00 90.00 90.00	58.84 58.84 151.21 90.00 90.00 90.00	58.85 58.85 151.26 90.00 90.00 90.00	58.83 58.83 151.27 90.00 90.00 90.00
Unit cell volume (Å^3)	522839	523511	523862.2	523540.8
Total reflections	686302 (30123)	587692 (29088)	480296 (22950)	389623 (17213)
Multiplicity	8.6 (7.9)	8.7 (8.6)	8.6 (8.6)	8.6 (8.0)
Mosaicity (°)	0.12	0.13	0.14	0.14
Completeness (%)	99.9 (98.6)	99.9 (98.1)	99.9 (98.0)	99.9 (97.9)
Mean I/sigma(I)	8.5 (0.5)	8.9 (0.5)	9.2 (0.5)	9.1 (0.6)
Wilson B-factor (Å^2)	20.9	23.7	26.6	28.7
R-merge	0.110 (4.479)	0.118 (5.270)	0.139 (7.530)	0.186 (9.560)
R-pim	0.040 (1.678)	0.042 (1.868)	0.050 (2.668)	0.066 (3.509)
$CC_{1/2}$	0.999 (0.304)	0.999 (0.302)	0.999 (0.320)	0.999 (0.335)
Isa	17.3	18.0	17.7	18.0

Thaumatin crystal structure refinement statistics			
Dataset	1		4

PDB code	7LFG		7LJV
Resolution range (Å)	37.79 - 1.22 (1.26 - 1.22)		37.82 - 1.48 (1.53 - 1.48)
Reflections used in refinement	78744 (6867)		43991 (3270)
Rwork	0.135 (0.320)		0.138 (0.303)
Rfree	0.150 (0.337)		0.169 (0.329)
# of non-hydrogen atoms	1957		1911
Protein	1764		1744
Ligand/ion	10		10
Water	165		143
RMS (bonds)	0.007		0.007
RMS (angles)	0.94		0.92
Average B-factor (Å^2)	21.77		26.59
Protein	20.2		25.34
Ligand/ion	17.85		23.44
Water	37.17		40.69
Ramachandran (%)			
Favored	98.1		98.1
Allowed	1.9		1.9
Outliers	0		0

Table S1 Thaumatin room temperature diffraction and traditional single conformation model refinement statistics. Diffraction statistics for increasingly damaged thaumatin datasets obtained at 277 K from a single crystal. Diffraction statistics are reported for datasets of 120° total rotations obtained from the same crystal orientation. Values in parenthesis are for the highest resolution shells. All statistics were obtained from *AIMLESS* (Evans & Murshudov, 2013), with the exception of $CC_{1/2}$, which was obtained

from *XSCALE* (Kabsch, 2010). Average diffraction weighted doses (DWD) were estimated using the program *RADDOSE-3D* (Zeldin, Brockhauser *et al.*, 2013; Zeldin, Gerstel *et al.*, 2013). Refinement statistics were obtained from *PHENIX* (*phenix.table_one*) using the final refined models and reflections file.

Proteinase K 277 K diffraction data collection statistics				
Batch	1	2	3	4
Wavelength (Å)	0.88557			
Resolution range (Å)	34.91-1.02 (1.04-1.02)	34.84-1.10 (1.12-1.10)	34.81-1.30 (1.32-1.30)	34.85-1.43 (1.45-1.43)
Average diffraction weighted dose (MGy)	0.006	0.023	0.041	0.058
Space group	$P4_32_12$			
Unit cell a (Å), b (Å), c (Å), α (°), β (°), γ (°)	67.82 67.82 101.86 90.00 90.00 90.00	67.71 67.71 101.60 90.00 90.00 90.00	67.65 67.65 101.52 90.00 90.00 90.00	67.71 67.71 101.65 90.00 90.00 90.00
Unit cell volume (Å^3)	468510.4	465799.8	464608.6	466029.1
Total reflections	822825 (28269)	695054 (23190)	480869 (17003)	379902 (16456)
Multiplicity	6.8 (4.9)	7.2 (5.0)	8.2 (6.0)	8.6 (7.7)
Mosaicity (°)	0.08	0.12	0.22	0.30
Completeness (%)	99.9 (98.3)	99.9 (98.7)	99.9 (98.9)	99.9 (98.8)
Mean I/sigma(I)	8.5 (0.9)	8.8 (0.8)	12.1 (0.7)	11.4 (0.6)
Wilson B-factor (Å^2)	12.2	14.7	20.8	24.6
R-merge	0.098 (1.720)	0.102 (1.946)	0.107 (2.646)	0.130 (3.551)
R-pim	0.038 (0.862)	0.039 (0.950)	0.039 (1.138)	0.047 (1.335)
$CC_{1/2}$	0.999 (0.359)	0.999 (0.319)	0.999 (0.306)	0.999 (0.320)
Isa	19.3	17.7	35.4	40.6

Proteinase K crystal structure refinement statistics			
Dataset	1		4

PDB code	7LN7		7LPT
Resolution range (Å)	33.91 - 1.02 (1.06 - 1.02)		34.85 - 1.43 (1.48 - 1.43)
Reflections used in refinement	120585 (11691)		44021 (4101)
Rwork	0.123 (0.283)		0.125 (0.269)
Rfree	0.138 (0.284)		0.162 (0.323)
# of non-hydrogen atoms	2817		2735
Protein	2477		2435
Ligand/ion	17		17
Water	287		283
RMS (bonds)	0.006		0.007
RMS (angles)	0.92		0.89
Average B-factor ($Å^2$)	11.81		19.87
Protein	9.73		17.87
Ligand/ion	37.12		52.69
Water	26.46		35.10
Ramachandran (%)			
Favored	97.1		96.4
Allowed	2.9		3.6
Outliers	0		0

Table S2 Proteinase K room temperature diffraction and traditional single conformation model refinement statistics. Diffraction statistics for increasingly damaged proteinase K datasets obtained at 277 K from a single crystal. Diffraction statistics are reported for datasets of 120° total rotations obtained from the same crystal orientation. Values in parenthesis are for the highest resolution shells. All statistics were obtained from *AIMLESS* (Evans & Murshudov, 2013), with the exception of $CC_{1/2}$, which was obtained

from *XSCALE* (Kabsch, 2010). Average diffraction weighted doses (DWD) were estimated using the program *RADDOSE-3D* (Zeldin, Brockhauser *et al.*, 2013; Zeldin, Gerstel *et al.*, 2013). Refinement statistics were obtained from *PHENIX* (*phenix.table_one*) using the final refined models and reflections file.

Lysozyme 277 K diffraction data collection statistics			
Batch	1	2	3
Wavelength (Å)	0.88557		
Resolution range (Å)	38.63-1.13 (1.15-1.13)	38.61-1.30 (1.32-1.30)	38.70-1.52 (1.55-1.52)
Average diffraction weighted dose (MGy)	0.017	0.069	0.121
Space group	$P4_32_12$		
Unit cell a (Å), b (Å), c (Å), α (°), β (°), γ (°)	77.26 77.26 37.31 90.00 90.00 90.00	77.22 77.22 37.19 90.00 90.00 90.00	77.40 77.40 37.21 90.00 90.00 90.00
Unit cell volume (Å^3)	222707.4	221761.3	222916.2
Total reflections	365238 (17155)	241397 (11737)	152376 (6153)
Multiplicity	8.5 (8.4)	8.6 (8.7)	8.5 (7.2)
Mosaicity (°)	0.14	0.25	0.37
Completeness (%)	99.9 (99.1)	99.9 (98.2)	99.9 (98.1)
Mean I/sigma(I)	12.4 (0.9)	14.3 (0.8)	12.7 (0.6)
Wilson B-factor (Å^2)	18.9	24.5	31.3
R-merge	0.072 (2.720)	0.077 (3.766)	0.102 (4.132)
R-pim	0.026 (0.989)	0.028 (1.356)	0.037 (1.620)
$CC_{1/2}$	0.999 (0.326)	0.999 (0.317)	0.999 (0.335)
Isa	20.1	25.7	28.9

Lysozyme crystal structure refinement statistics			
Dataset	1		3
PDB code	7LLP		7LN8
Resolution range (Å)	33.6 - 1.13 (1.17 - 1.13)		33.53 - 1.52 (1.58 - 1.52)
Reflections used in refinement	42596 (4064)		17663 (1565)
Rwork	0.132 (0.292)		0.139 (0.261)
Rfree	0.155 (0.313)		0.200 (0.375)
# of non-hydrogen atoms	1383		1367
Protein	1247		1247
Ligand/ion	3		3
Water	116		102
RMS (bonds)	0.008		0.008
RMS (angles)	0.99		0.91
Average B-factor ($Å^2$)	20.3		26.99
Protein	19.1		26.02
Ligand/ion	28.83		39.18
Water	31.44		37.04
Ramachandran (%)			
Favored	99.2		100
Allowed	0.8		0
Outliers	0		0

Table S3 Lysozyme room temperature diffraction and traditional single conformation model refinement statistics. Diffraction statistics for increasingly damaged lysozyme datasets obtained at 277 K from a single crystal. Diffraction statistics are reported for datasets of 120° total rotations obtained from the same crystal orientation. Values in parenthesis are for the highest resolution shells. All statistics were obtained from *AIMLESS* (Evans & Murshudov, 2013), with the exception of $CC_{1/2}$, which was obtained from *XSCALE* (Kabsch, 2010). Average diffraction weighted doses (DWD) were estimated using the program *RADDOSE-3D* (Zeldin, Brockhauser *et al.*, 2013; Zeldin, Gerstel *et al.*, 2013). Refinement statistics were obtained from *PHENIX* (*phenix.table_one*) using the final refined models and reflections file.

Lysozyme 277 K diffraction data collection statistics		
Batch	Crystal 1 dataset 1	Crystal 2 dataset 1
Wavelength (Å)	0.88557	0.88557
Resolution range (Å)	38.63-1.13 (1.15-1.13)	38.70-1.10 (1.12-1.10
Dose (MGy) [a]	0.058	0.029
Space group	$P4_32_12$	$P4_32_12$
Unit cell a (Å), b (Å), c (Å), α (°), β (°), γ (°)	77.26 77.26 37.31 90.00 90.00 90.00	77.41 77.41 37.42 90.00 90.00 90.00
Unit cell volume ($Å^3$)	222707.4	224232.2
Total reflections	365238 (17155)	399774 (18647)
Multiplicity	8.5 (8.4)	8.6 (8.4)
Mosaicity (°)	0.14	0.08
Completeness (%)	99.9 (99.1)	99.3 (98.3)
Mean I/sigma(I)	12.4 (0.9)	9.8 (0.7)
Wilson B-factor ($Å^2$)	18.9	17.6
R-merge	0.072 (2.720)	0.083 (2.940)
R-pim	0.026 (0.989)	0.029 (1.066)
$CC_{1/2}$	0.999 (0.326)	0.999 (0.302)
Isa	20.1	19.5
Lysozyme multi-conformer model refinement statistics		
Dataset	1	1
PDB code	7LN9	7LPM
Resolution range (Å)	33.6 - 1.13 (1.171 - 1.13)	34.62 - 1.1 (1.14 - 1.1)

Reflections used in refinement	42596 (4064)	46101 (4434)
Rwork	0.136 (0.292)	0.136 (0.292)
Rfree	0.156 (0.308)	0.158 (0.301)
# of non-hydrogen atoms	3065	3125
Protein	2925	2984
Ligand/ion	4	4
Water	116	112
RMS (bonds)	0.006	0.006
RMS (angles)	0.84	0.81
Average B-factor (Å^2)	15.8	15.14
Protein	15.2	14.55
Ligand/ion	22.25	22.14
Water	28.48	27.8
Ramachandran (%)		
Favored	96.1	96.1
Allowed	3.9	3.9
Outliers	0	0

Table S4 Room temperature (277K) diffraction statistics and multi-conformer refinement statistics for two lysozyme crystals. Diffraction statistics are reported for datasets of 120° total rotations. Values in parenthesis are for the highest resolution shells. All statistics were obtained from *AIMLESS* (Evans & Murshudov, 2013), with the exception of $CC_{1/2}$, which was obtained from *XSCALE* (Kabsch, 2010). Average diffraction weighted doses (DWD) were estimated using the program *RADDOSE-3D* (Zeldin, Brockhauser *et al.*, 2013; Zeldin, Gerstel *et al.*, 2013). Multi-conformer models were obtained as described in Materials and Methods. Refinement statistics were obtained from *PHENIX* (*phenix.table_one*) using the final refined models and reflections files. Diffraction statistics for crystal 1 are from Table S3 dataset 1.

Thaumatin refinement statistics multi-conformer models				
Dataset	1	2	3	4
PDB code	7LJW	7LJZ	7LK5	7LK6
Resolution range (Å)	38.26 -1.22 (1.26 -1.22)	37.8 - 1.29 (1.33 - 1.29)	37.82 - 1.38 (1.43 - 1.38)	37.82 - 1.48 (1.53 - 1.48)
Reflections used in refinement	78731 (6867)	66525 (5655)	54141 (4338)	43991 (3270)
Rwork	0.142 (0.332)	0.1444 (0.335)	0.146 (0.348)	0.146 (0.317)
Rfree	0.156 (0.340)	0.1600 (0.338)	0.166 (0.387)	0.169 (0.335)
# of non-hydrogen atoms	3771	3766	3766	3764
Protein	3578	3578	3578	3578
Ligand/ion	20	20	20	20
Water	151	148	148	143
RMS (bonds)	0.009	0.009	0.009	0.009
RMS (angles)	1.06	1.08	1.08	1.07
Average B-factor ($Å^2$)	18.18	19.64	21.62	22.49
Protein	17.48	18.95	20.93	21.84
Ligand/ion	16.13	16.95	18.02	19.51
Water	32.85	34.57	36.57	36.85
Ramachandran (%)				
Favored	96.6	96.1	95.1	94.6
Allowed	3.4	3.9	4.9	5.4
Outliers	0	0	0	0

Table S5 Refinement statistics for multi-conformer thaumatin models obtained from increasingly damaged datasets from a single crystal at room temperature (277 K). Multi-conformer models were refined as described in Materials and Methods and using diffraction datasets from Table S1. Refinement statistics were obtained from *PHENIX* (*phenix.table_one*) using the final refined models and reflections file.

Proteinase K refinement statistics multi-conformer models				
Dataset	1	2	3	4
PDB code	7LPU	7LPV	7LQ8	7LQ9
Resolution range (Å)	33.91 - 1.02 (1.06 - 1.02)	32.12 - 1.1 (1.14 - 1.1)	33.83 - 1.301 (1.35 - 1.301)	34.85 - 1.43 (1.48 - 1.43)
Reflections used in refinement	120585 (11691)	95793 (9247)	58149 (5476)	44021 (4101)
Rwork	0.119 (0.287)	0.123 (0.285)	0.121 (0.294)	0.124 (0.272)
Rfree	0.138 (0.301)	0.146 (0.289)	0.151 (0.322)	0.162 (0.317)
# of non-hydrogen atoms	6724	6723	6676	6676
Protein	6345	6345	6312	6312
Ligand/ion	22	22	22	22
Water	282	281	265	263
RMS (bonds)	0.007	0.007	0.007	0.007
RMS (angles)	0.95	0.95	0.92	0.92
Average B-factor ($Å^2$)	8.97	10.96	13.61	16.33
Protein	8.1	10.05	12.76	15.46
Ligand/ion	22.93	25.63	30.83	35.33
Water	23.57	26.29	28.23	31.12
Ramachandran (%)				
Favored	96.03	95.67	95.67	94.95
Allowed	3.97	4.33	4.33	5.05
Outliers	0	0	0	0

Table S6 Refinement statistics for multi-conformer proteinase K models obtained from increasingly damaged datasets from a single crystal at room temperature (277 K). Multi-conformer models were refined as described in Materials and Methods and using diffraction datasets from Table S2. Refinement statistics were obtained from *PHENIX* (*phenix.table_one*) using the final refined models and reflections file.

Lysozyme refinement statistics multi-conformer models			
Dataset	1	2	3
PDB code	7LN9	7LOQ	7LOR
Resolution range (Å)	33.6 - 1.13 (1.171 - 1.13)	34.54 - 1.301 (1.348 - 1.301)	33.53 - 1.522 (1.576 - 1.522)
Reflections used in refinement	42596 (4064)	27852 (2526)	17663 (1565)
Rwork	0.136 (0.292)	0.138 (0.318)	0.145 (0.290)
Rfree	0.156 (0.308)	0.167 (0.347)	0.197 (0.396)
# of non-hydrogen atoms	3065	3065	3051
Protein	2925	2925	2925
Ligand/ion	4	4	4
Water	113	113	102
RMS (bonds)	0.006	0.006	0.005
RMS (angles)	0.84	0.82	0.75
Average B-factor ($Å^2$)	15.8	17.81	22.5
Protein	15.2	17.19	22.01
Ligand/ion	22.25	25.1	30.13
Water	28.48	30.79	34.02
Ramachandran (%)			
Favored	96.06	93.7	95.28
Allowed	3.94	6.3	4.72
Outliers	0	0	0

Table S7 Refinement statistics for multi-conformer lysozyme models obtained from increasingly damaged datasets from a single crystal at room temperature (277 K). Multi-conformer models were refined as described in Materials and Methods and using diffraction datasets from Table S3. Refinement statistics were obtained from *PHENIX* (*phenix.table_one*) using the final refined models and reflections file.

Thaumatin 277 K diffraction data collection statistics				
Dataset	1	2 (merged)	3 (merged)	4 (merged)
Wavelength (Å)	0.88557			
Resolution range (Å)	38-26-1.22 (1.24-1.22)	38-27-1.22 (1.24-1.22)	38-27-1.22 (1.24-1.22)	38-27-1.22 (1.24-1.22)
DWD (MGy)	0.016	0.114	0.212	0.310
Space group	$P4_12_12$			
Unit cell a (Å), b (Å), c (Å), α (°), β (°), γ (°)	58.81 58.81 151.17 90.00 90.00 90.00	58.82 58.82 151.15 90.00 90.00 90.00	58.82 58.82 151.16 90.00 90.00 90.00	58.82 58.82 151.17 90.00 90.00 90.00
Unit cell volume ($Å^3$)	522839.0	522947.6	522982.2	523016.8
Total reflections	686302 (30123)	4818222 (209908)	8948567 (403085)	13072934 (568854)
Multiplicity	8.6 (7.9)	60.0 (54.3)	112.0 (100.5)	163.6 (146.5)
Mosaicity (°)	0.12	0.12	0.12	0.13
Completeness (%)	99.9 (98.6)	100 (99.5)	100 (99.5)	100 (99.8)
Mean I/sigma(I)	8.5 (0.5)	21.5 (1.1)	26.6 (1.2)	28.5 (1.1)
Wilson B-factor ($Å^2$)	20.9	21.8	22.6	23.0
R-merge	0.110 (4.479)	0.135 (6.955)	0.206 (16.249)	0.459 (58.722)
R-pim	0.040 (1.678)	0.018 (0.938)	0.019 (1.605)	0.036 (4.793)
$CC_{1/2}$	0.999 (0.304)	1.000 (0.65.7)	1.000 (0.666)	1.000 (0.587)
Isa	17.3	16.1	15.5	15.2
Thaumatin refinement statistics multi-conformer models				
Dataset	1	2 (merged)	3 (merged)	4 (merged)
PDB code	7LJW	7LNB	7LNC	7LND
Resolution range (Å)	38.26 -1.22 (1.26 -1.22)	37.79 - 1.22 (1.26 - 1.22)	38.27 - 1.22 (1.26 - 1.22)	36.41 - 1.22 (1.26 - 1.22)

Reflections used in refinement	78731 (6867)	79672 (7713)	79668 (7721)	79570 (7758)
Rwork	0.142 (0.332)	0.133 (0.274)	0.136 (0.269)	0.136 (0.300)
Rfree	0.156 (0.340)	0.145 (0.284)	0.147 (0.272)	0.148 (0.309)
# of non-hydrogen atoms	3771	3771	3771	3771
Protein	3578	3578	3578	3578
Ligand/ion	20	20	20	20
Water	151	151	151	151
RMS (bonds)	0.009	0.009	0.006	0.009
RMS (angles)	1.06	1.06	0.91	1.07
Average B-factor ($Å^2$)	18.18	18.14	18.48	20.89
Protein	17.48	17.45	17.79	20.19
Ligand/ion	16.13	15.56	15.63	17.97
Water	32.85	32.81	33.14	35.52
Ramachandran (%)				
Favored	96.6	96.1	96.1	96.1
Allowed	3.4	3.9	3.9	3.9
Outliers	0	0	0	0

Table S8 Room temperature (277 K) diffraction statistics and multi-conformer refinement statistics for increasingly damaged thaumatin datasets. Diffraction statistics are reported for increasingly damaged datasets in which an increasing amount of increasingly damaged data have been merged together –i.e. dataset 1 is of 120° total rotation, dataset 2 is of 480° total rotation and so forth. Values in parenthesis are for the highest resolution shells. All diffraction statistics were obtained from *AIMLESS* (Evans & Murshudov, 2013), with the exception of $CC_{1/2}$, which was obtained from *XSCALE* (Kabsch, 2010). Average diffraction weighted doses (DWD) were estimated using the program *RADDOSE-3D* (Zeldin, Brockhauser *et al.*, 2013; Zeldin, Gerstel *et al.*, 2013). Multi-conformer models were obtained as described in Materials and Methods. Refinement statistics were obtained from *PHENIX* (*phenix.table_one*) using the final refined models and reflections files. Diffraction and refinement statistics for dataset 1 and the respective multi-conformer model are from Table S1 and Table S5, respectively.

Proteinase K 277 K diffraction data collection statistics				
Dataset	1	2 (merged)	3 (merged)	4 (merged)
Wavelength (Å)	0.88557			
Resolution range (Å)	34.91-1.02 (1.04-1.02)	34.89-1.02 (1.04-1.02)	34.88-1.02 (1.04-1.02)	34.89-1.02 (1.04-1.02)
DWD (MGy)	0.006	0.023	0.041	0.058
Space group	$P4_32_12$			
Unit cell a (Å), b (Å), c (Å), α (°), β (°), γ (°)	67.82 67.82 101.86 90.00 90.00 90.00	67.78 67.78 101.76 90.00 90.00 90.00	67.77 67.77 101.76 90.00 90.00 90.00	67.78 67.78 101.78 90.00 90.00 90.00
Unit cell volume ($Å^3$)	468510.4	467498.5	467360.6	467590.4
Total reflections	822825 (28269)	3282233 (111354)	5727309 (192083)	8153634 (270403)
Multiplicity	6.8 (4.9)	27.2 (19.0)	47.5 (32.7)	67.6 (46.1)
Mosaicity (°)	0.08	0.09	0.13	0.18
Completeness (%)	99.9 (98.3)	100 (100)	100 (100)	100 (100)
Mean I/sigma(I)	8.5 (0.9)	14.4 (1.2)	16.7 (1.2)	17.7 (1.2)
Wilson B-factor ($Å^2$)	12.2	13.0	13.7	14.2
R-merge	0.098 (1.720)	0.133 (3.410)	0.248 (12.902)	0.625 (55.751)
R-pim	0.038 (0.862)	0.025 (0.792)	0.037 (2.232)	0.082 (8.158)
$CC_{1/2}$	0.999 (0.359)	1.000 (0.544)	1.000 (0.477)	1.000 (0.442)
Isa	19.3	14.8	14.9	15.2
Proteinase K refinement statistics multi-conformer models				
Dataset	1	2 (merged)	3 (merged)	4 (merged)
PDB code	7LPU	7LQA	7LQB	7LQC
Resolution range (Å)	33.91 - 1.02 (1.06 - 1.02)	33.89 - 1.02 (1.06 - 1.02)	33.89 - 1.02 (1.06 - 1.02)	33.92 - 1.021 (1.06 - 1.021)

Reflections used in refinement	120585 (11691)	120536 (11840)	120501 (11846)	120548 (11846)
Rwork	0.119 (0.287)	0.110 (0.241)	0.111 (0.243)	0.111 (0.277)
Rfree	0.138 (0.301)	0.127 (0.257)	0.128 (0.261)	0.128 (0.285)
# of non-hydrogen atoms	6724	6724	6724	6724
Protein	6345	6345	6345	6345
Ligand/ion	22	22	22	22
Water	282	282	281	281
RMS (bonds)	0.007	0.007	0.007	0.007
RMS (angles)	0.95	0.96	0.96	0.96
Average B-factor ($Å^2$)	8.97	8.9	8.83	10.71
Protein	8.1	8.04	7.96	9.83
Ligand/ion	22.93	22.43	22.12	24.26
Water	23.57	23.52	23.45	25.5
Ramachandran (%)				
Favored	96.03	95.67	95.67	96.75
Allowed	3.97	4.33	4.33	3.25
Outliers	0	0	0	0

Table S9 Room temperature (277K) diffraction statistics and multi-conformer refinement statistics for increasingly damaged proteinase K datasets. Diffraction statistics are reported for increasingly damaged datasets in which an increasing amount of increasingly damaged data have been merged together –i.e. dataset 1 is of 120° total rotation, dataset 2 is of 480° total rotation and so forth. Values in parenthesis are for the highest resolution shells. All diffraction statistics were obtained from *AIMLESS* (Evans & Murshudov, 2013), with the exception of $CC_{1/2}$, which was obtained from *XSCALE* (Kabsch, 2010). Average diffraction weighted doses (DWD) were estimated using the program *RADDOSE-3D* (Zeldin, Brockhauser *et al.*, 2013; Zeldin, Gerstel *et al.*, 2013). Multi-conformer models were obtained as described in Materials and Methods. Refinement statistics were obtained from *PHENIX* (*phenix.table_one*) using the final refined models and reflections files. Diffraction and refinement statistics for dataset 1 and the respective multi-conformer model are from Table S2 and Table S6, respectively.

Lysozyme 277 K diffraction data collection statistics			
Dataset	1	2 (merged)	3 (merged)
Wavelength (Å)	0.88557		
Resolution range (Å)	38.63-1.13 (1.15-1.13)	38.63-1.13 (1.15-1.13)	38.60-1.14 (1.16-1.14)
DWD (MGy)	0.017	0.069	0.121
Space group	$P4_32_12$		
Unit cell a (Å), b (Å), c (Å), α (°), β (°), γ (°)	77.26 77.26 37.31 90.00 90.00 90.00	77.25 77.25 37.27 90.00 90.00 90.00	77.20 77.20 37.28 90.00 90.00 90.00
Unit cell volume ($Å^3$)	222707.4	222411.0	222182.8
Total reflections	365238 (17155)	1455624 (67426)	2468785 (105094)
Multiplicity	8.5 (8.4)	34.0 (32.7)	59.2 (51.7)
Mosaicity (°)	0.14	0.2	0.26
Completeness (%)	99.9 (99.1)	100.0 (99.9)	100.0 (100.0)
Mean I/sigma(I)	12.4 (0.9)	20.1 (1.1)	19.3 (1.1)
Wilson B-factor ($Å^2$)	18.9	20.1	21.0
R-merge	0.072 (2.720)	0.119 (7.926)	0.411 (56.454)
R-pim	0.026 (0.989)	0.021 (1.382)	0.054 (7.853)
$CC_{1/2}$	0.999 (0.326)	1.000 (0.419)	1.000 (0.388)
Isa	20.1	19.9	17.7
Lysozyme refinement statistics multi-conformer models			
Dataset	1	2 (merged)	3 (merged)
PDB code	7LN9	7LP6	7LPL
Resolution range (Å)	33.6 - 1.13 (1.171 - 1.13)	38.63 - 1.13 (1.17 - 1.13)	33.56 - 1.14 (1.18 - 1.14)
Reflections used in refinement	42596 (4064)	42724 (4176)	41595 (4012)

Rwork	0.136 (0.292)	0.136 (0.269)	0.137 (0.304)
Rfree	0.156 (0.308)	0.156 (0.273)	0.158 (0.301)
# of non-hydrogen atoms	3065	3065	3065
Protein	2925	2925	2925
Ligand/ion	4	4	4
Water	113	113	113
RMS (bonds)	0.006	0.007	0.006
RMS (angles)	0.84	0.87	0.85
Average B-factor (Å^2)	15.8	15.73	17.33
Protein	15.2	15.14	16.72
Ligand/ion	22.25	22.37	24.02
Water	28.48	28.31	30.12
Ramachandran (%)			
Favored	96.06	96.06	95.28
Allowed	3.94	3.94	4.72
Outliers	0	0	0

Table S10 Room temperature (277K) diffraction statistics and multi-conformer refinement statistics for increasingly damaged lysozyme datasets. Diffraction statistics are reported for increasingly damaged datasets in which an increasing amount of increasingly damaged data have been merged together –i.e. dataset 1 is of 120° total rotation, dataset 2 is of 480° total rotation and so forth. Values in parenthesis are for the highest resolution shells. All diffraction statistics were obtained from *AIMLESS* (Evans & Murshudov, 2013), with the exception of $CC_{1/2}$, which was obtained from *XSCALE* (Kabsch, 2010). Average diffraction weighted doses (DWD) were estimated using the program *RADDOSE-3D* (Zeldin, Brockhauser *et al.*, 2013; Zeldin, Gerstel *et al.*, 2013). Multi-conformer models were obtained as described in Materials and Methods. Refinement statistics were obtained from *PHENIX* (*phenix.table_one*) using the final refined models and reflections files. Diffraction and refinement statistics for dataset 1 and the respective multi-conformer model are from Table S3 and Table S7, respectively.

Proteinase K 100 K diffraction data collection statistics							
Dataset	1	2	3	4	5	6	7
Wavelength (Å)	0.88557						
Resolution range (Å)	34.82-0.90 (0.92-0.90)	34.82-0.91 (0.93-0.91)	34.84-0.95 (0.97-0.95)	34.84-1.01 (1.03-1.01)	34.86-1.06 (1.08-1.06)	34.86-1.11 (1.13-1.11)	34.86-1.16 (1.18-1.16)
Dose (MGy)	0.3	2.1	3.9	5.7	7.5	9.3	11.0
Space group	$P4_32_12$						
Unit cell a (Å) b (Å) c (Å) α (°) β (°) γ (°)	67.72 67.72 101.42 90.00 90.00 90.00	67.74 67.74 101.52 90.00 90.00 90.00	67.75 67.75 101.55 90.00 90.00 90.00	67.75 67.75 101.62 90.00 90.00 90.00	67.75 67.75 101.65 90.00 90.00 90.00	67.76 67.76 101.70 90.00 90.00 90.00	67.73 67.73 101.66 90.00 90.00 90.00
Unit cell volume ($Å^3$)	465112	465845.6	466120.8	466442.2	466579.9	466947.2	466350.3
Total reflections	1196300 (17467)	1184687 (19176)	1113598 (31210)	993533 (29085)	895131 (32249)	799556 (33561)	702050 (32297)
Multiplicity	6.9 (2.2)	7.1 (2.9)	7.5 (4.4)	8.0 (5.1)	8.3 (6.2)	8.5 (7.3)	8.5 (8.2)
Mosaicity (°)	0.18	0.19	0.19	0.19	0.19	0.19	0.19
Completeness (%)	99.6 (93.0)	99.9 (81.1)	99.9 (98.5)	99.8 (95.7)	100.0 (99.5)	100.0 (99.9)	99.9 (98.0)
Mean I/sigma(I)	10.3 (1.0)	10.4 (0.5)	11.2 (0.6)	11.8 (0.6)	10.5 (0.7)	12.7 (0.7)	12.7 (0.7)
Wilson B-factor ($Å^2$)	9.8	11.5	12.7	14.7	16.6	18.8	21.3
R-merge	0.076 (0.716)	0.073 (1.436)	0.073 (2.014)	0.062 (1.965)	0.067 (2.426)	0.061 (2.412)	0.061 (2.815)

R-pim	0.029 (0.519)	0.028 (0.922)	0.027 (1.055)	0.023 (0.922)	0.024 (1.035)	0.022 (0.941)	0.022 (1.033)
$CC_{1/2}$	1.000 (0.604)	1.000 (0.364)	1.000 (0.306)	1.000 (0.324)	1.000 (0.340)	1.000 (0.346)	1.000 (0.312)
Isa	20.7	21.1	24.0	25.4	26.4	28.7	31.0
Proteinase K crystal structure refinement statistics							
PDB code	7LTD	7LTI	7LTV	7LU0	7LU1	7LQC	7LU3
Resolution range (Å)	32.12 - 0.9 (0.93 - 0.90)	32.12 - 0.91 (0.94 - 0.91)	32.13 - 0.95 (0.98 - 0.95)	33.88 - 1.01 (1.05 - 1.01)	33.88 - 1.06 (1.10 - 1.06)	32.14 - 1.11 (1.15 - 1.11)	33.87 - 1.16 (1.20 - 1.16)
Reflections used in refinement	173034 (16402)	165151 (13733)	147039 (13382)	122587 (10937)	106888 (10055)	93318 (8735)	81806 (7794)
Rwork	0.157 (0.298)	0.153 (0.315)	0.150 (0.308)	0.146 (0.321)	0.144 (0.3003)	0.145 (0.291)	0.141 (0.305)
Rfree	0.172 (0.310)	0.170 (0.314)	0.170 (0.314)	0.168 (0.323)	0.169 (0.313)	0.173 (0.301)	0.172 (0.311)
# of non-hydrogen atoms	3078	3070	3049	3004	2946	2850	2786
Protein	2492	2524	2555	2541	2533	2495	2473
Ligand/ion	21	21	21	21	17	13	13
Water	461	428	395	376	334	292	267
RMS (bonds)	0.005	0.006	0.006	0.006	0.006	0.007	0.007
RMS (angles)	0.9	0.9	0.89	0.89	0.89	0.89	0.89
Average B-factor ($Å^2$)	9.99	12.07	13.53	15.2	17.72	19.65	21.92
Protein	7.47	9.58	11.01	12.87	15.32	17.58	19.67
Ligand/ion	20.34	27.69	36.59	35.5	52.25	49.43	46.69
Water	20.73	23.42	26.16	27.63	31.61	33.59	39.39

Ramachandran (%)							
Favored	97.47	97.47	97.47	97.47	97.11	97.11	97.11
Allowed	2.53	2.53	2.17	2.17	2.53	2.53	2.53
Outliers	0	0	0.36	0.36	0.36	0.36	0.36

Table S11 Diffraction data collection and refinement statistics for increasingly X-ray damaged proteinase K datasets obtained from a single cryo-cooled (100 K) crystal. Diffraction statistics are reported for increasingly damaged dataset, each of 120° total rotation. Values in parenthesis are for the highest resolution shells. All diffraction statistics were obtained from *AIMLESS* (Evans & Murshudov, 2013), with the exception of $CC_{1/2}$, which was obtained from *XSCALE* (Kabsch, 2010). Average diffraction weighted doses (DWD) were estimated using the program *RADDOSE-3D* (Zeldin, Brockhauser *et al.*, 2013; Zeldin, Gerstel *et al.*, 2013). Structural models were obtained in a highly consistent manner and as described in Materials and Methods. Refinement statistics were obtained from *PHENIX* (*phenix.table_one*) using the final refined models and reflections files.

277 K crystal	**100 K crystal**
T4	S138
T22	S139
S61	S140
S63	R185
D97	T244
S101	S247
R167	

Table S12 Proteinase K residues the side chains of which are in contact with crystallization components within the crystal.

References

Adam, V., Carpentier, P., Violot, S., Lelimousin, M., Darnault, C., Nienhaus, G. U. & Bourgeois, D. (2009). *J. Am. Chem. Soc.* **131**, 18063–18065.

Burmeister, W. P. (2000). *Acta Crystallogr. D Biol. Crystallogr.* **56**, 328–341.

Carugo, O. & Carugo, K. D. (2005). *Trends Biochem. Sci.* **30**, 213–219.

Chapman, H. N., Fromme, P., Barty, A., White, T. A., Kirian, R. A., Aquila, A., Hunter, M. S., Schulz, J., DePonte, D. P., Weierstall, U., Doak, R. B., Maia, F. R. N. C., Martin, A. V., Schlichting, I., Lomb, L., Coppola, N., Shoeman, R. L., Epp, S. W., Hartmann, R., Rolles, D., Rudenko, A., Foucar, L., Kimmel, N., Weidenspointner, G., Holl, P., Liang, M., Barthelmess, M., Caleman, C., Boutet, S., Bogan, M. J., Krzywinski, J., Bostedt, C., Bajt, S., Gumprecht, L., Rudek, B., Erk, B., Schmidt, C., Hömke, A., Reich, C., Pietschner, D., Strüder, L., Hauser, G., Gorke, H., Ullrich, J., Herrmann, S., Schaller, G., Schopper, F., Soltau, H., Kühnel, K.-U., Messerschmidt, M., Bozek, J. D., Hau-Riege, S. P., Frank, M., Hampton, C. Y., Sierra, R. G., Starodub, D., Williams, G. J., Hajdu, J., Timneanu, N., Seibert, M. M., Andreasson, J., Rocker, A., Jönsson, O., Svenda, M., Stern, S., Nass, K., Andritschke, R., Schröter, C.-D., Krasniqi, F., Bott, M., Schmidt, K. E., Wang, X., Grotjohann, I., Holton, J. M., Barends, T. R. M., Neutze, R., Marchesini, S., Fromme, R., Schorb, S., Rupp, D., Adolph, M., Gorkhover, T., Andersson, I., Hirsemann, H., Potdevin, G., Graafsma, H., Nilsson, B. & Spence, J. C. H. (2011). *Nature*. **470**, 73–77.

Coquelle, N., Brewster, A. S., Kapp, U., Shilova, A., Weinhausen, B., Burghammer, M. & Colletier, J. P. (2015). *Acta Crystallogr. D Biol. Crystallogr.* **71**, 1184–1196.

Dauter (1999). *Acta Crystallogr. D Biol. Crystallogr.* **55**, 1703–1717.

Dauter (2017). *Protein Crystallography: Methods and Protocols*, Vol. edited by Wlodawer, Dauter & Jaskolski, pp. 165–184. New York, NY: Springer.

Doerr, A. (2011). *Nat. Methods*. **8**, 283–283.

Evans & Murshudov (2013). *Acta Crystallogr. D Biol. Crystallogr.* **69**, 1204–1214.

Fioravanti, E., Vellieux, F. M. D., Amara, P., Madern, D. & Weik, M. (2007). *J. Synchrotron Radiat.* **14**, 84–91.

Garman, E. F. (2010). *Acta Crystallogr. D Biol. Crystallogr.* **66**, 339–351.

Gotthard, G., Aumonier, S., De Sanctis, D., Leonard, G., von Stetten, D. & Royant, A. (2019). *IUCrJ*. **6**, 665–680.

Holton, J. M. (2009). *J. Synchrotron Radiat.* **16**, 133–142.

Kabsch, W. (2010). *Acta Crystallogr. D Biol. Crystallogr.* **66**, 125–132.

Keedy, D. A., Kenner, L. R., Warkentin, M., Woldeyes, R. A., Hopkins, J. B., Thompson, M. C., Brewster, A. S., Van Benschoten, A. H., Baxter, E. L., Uervirojnangkoorn, M., McPhillips, S. E., Song, J., Alonso-Mori, R., Holton, J. M., Weis, W. I., Brunger, A. T., Soltis, S. M., Lemke, H., Gonzalez, A., Sauter, N. K., Cohen, A. E., van den Bedem, H., Thorne, R. E. & Fraser, J. S. (2015). *ELife*. **4**, e07574.

Kort, R., Hellingwerf, K. J. & Ravelli, R. B. G. (2004). *J. Biol. Chem.* **279**, 26417–26424.

Leiros, H. K., McSweeney, S. M. & Smalås, A. O. (2001). *Acta Crystallogr. D Biol. Crystallogr.* **57**, 488–497.

Lewandowski, J. R., Halse, M. E., Blackledge, M. & Emsley, L. (2015). *Science*. **348**, 578–581.

Matsui, Y., Sakai, K., Murakami, M., Shiro, Y., Adachi, S. ichi, Okumura, H. & Kouyama, T. (2002). *J. Mol. Biol.* **324**, 469–481.

de la Mora, E., Coquelle, N., Bury, C. S., Rosenthal, M., Holton, J. M., Carmichael, I., Garman, E. F., Burghammer, M., Colletier, J.-P. & Weik, M. (2020). *Proc. Natl. Acad. Sci. U. S. A.* **117**, 4142–4151.

Nave, C. & Garman, E. (2005). *J. Synchrotron Radiat.* **12**, 257–260.

Neutze, R., Wouts, R. & Hajdu, J. (2000). **406**, 6.

Ravelli, R. B. & McSweeney, S. M. (2000). *Struct. Lond. Engl. 1993*. **8**, 315–328.

Ringe, D. & Petsko, G. A. (2003). *Biophys. Chem.* **105**, 667–680.

Roedig, P., Duman, R., Sanchez-Weatherby, J., Vartiainen, I., Burkhardt, A., Warmer, M., David, C., Wagner, A. & Meents, A. (2016). *J. Appl. Crystallogr.* **49**, 968–975.

Russi, S., González, A., Kenner, L. R., Keedy, D. A., Fraser, J. S. & van den Bedem, H. (2017). *J. Synchrotron Radiat.* **24**, 73–82.

Sjöblom, B., Polentarutti, M. & Djinović-Carugo, K. (2009). *Proc. Natl. Acad. Sci.* **106**, 10609–10613.

Southworth-Davies, R. J., Medina, M. A., Carmichael, I. & Garman, E. F. (2007). *Structure*. **15**, 1531–1541.

Taberman, H., Bury, C. S., van der Woerd, M. J., Snell, E. H. & Garman, E. F. (2019). *J. Synchrotron Radiat.* **26**, 931–944.

Tilton, R. F., Dewan, J. C. & Petsko, G. A. (1992). *Biochemistry*. **31**, 2469–2481.

Warkentin, M., Badeau, R., Hopkins, J. & Thorne, R. (2011). *Acta Crystallogr. Sect. D*. **67**, 792–803.

Warkentin, M., J.b, H., R.e, T. & Badeau (2012). *Acta Crystallogr. Sect. D*. **68**, 1108–1117.

Warkentin, M. & Thorne, R. (2010). *Acta Crystallogr. Sect. D*. **66**, 1092–1100.

Weik, M., Bergès, J., Raves, M. L., Gros, P., McSweeney, S., Silman, I., Sussman, J. L., Houée-Levin, C. & Ravelli, R. B. G. (2002). *J. Synchrotron Radiat.* **9**, 342–346.

Weik, M., Ravelli, R. B. G., Kryger, G., McSweeney, S., Raves, M. L., Harel, M., Gros, P., Silman, I., Kroon, J. & Sussman, J. L. (2000). *Proc. Natl. Acad. Sci.* **97**, 623–628.

Zeldin, O. B., Brockhauser, S., Bremridge, J., Holton, J. M. & Garman, E. F. (2013). *Proc. Natl. Acad. Sci. U. S. A.* **110**, 20551–20556.

Zeldin, O. B., Gerstel, M. & Garman, E. F. (2013). *J. Appl. Crystallogr.* **46**, 1225–1230.